Project Code: RWT-0910

PURIFICATION OF LIGHT ALCOHOLS USING MACROPOROUS HYDROPHOBIC MEMBRANES

A Major Qualifying Project Report:
Submitted to the Faculty
of the
WORCESTER POLYTECHNIC INSTITUTE
In partial fulfillment of the requirements for the
Degree of Bachelor of Science
April 29, 2010
By:

Adam Brooks

Anthony Laine

Patrick O'Brien

Professor Robert W. Thompson, Advisor

1 Abstract

The need for cheap and renewable energy has led to research into developing new technologies. While fossil fuel as an energy source is not leaving overnight, the transitional movement to alternative fuels has begun. Ethanol is one fuel that will likely play a leading role as a future energy source. However, great production energy requirements presently exist with the separation of ethanol from water, limiting overall energy output and emissions reductions. Membrane separation was studied using macroporous hydrophobic polymers in thin film discs. It was witnessed, despite zero mass flux with pure water feed, that this separation method offers no selectivity in alcohol-water mixtures. In addition, an investigation was made to simulate the phase existence within the pores.

2 Executive Summary

With energy consumption in the transportation sector continuously increasing, the political climate towards renewable energy sources has become a topic of much consideration. Finite energy resources, particularly petroleum and its derivative gasoline, are used today in way that is not sustainable while also extensively emitting greenhouse gases. Lighter-weight alcohols are currently being employed in the energy sector, prominently ethanol as an oxygenate source as a gasoline additive. This marks a step in the right direction, but there are limitations to these fuels.

The energy return-on-investment for ethanol shows that a substantial amount of non-renewable fossil fuel energy is used in the production of transportation-grade ethanol, rendering the fuel just about energy-neutral. In other words, there is approximately the same amount of energy required to produce and purify the compound as there is in the combustion energy output. This is caused by a number of aspects in the ethanol production process. Distillation and molecular sieve separation, the current separation benchmark, combine for the most significant energy investment of the production process. However new developments in membrane technologies, particularly with hydrophobic/hydrophilic characteristics, have shown to selectively transfer alcohol-water mixtures. This could potentially alleviate the energy costs of the separation, and became the focus of this MQP.

Several simple initial tests were performed to test the hydrophobicity of the membranes. Firstly contact angles were performed with both pure water and anhydrous ethanol. It was found that ethanol wets out while the distilled water beads up with contact angles of over 140

degrees for each of the three membrane materials and all pore sizes. Simple flux tests were also performed with pure feeds of water and ethanol. It was shown that the pure ethanol fluxes completely through the membrane while pure water is held back and is impervious to the membrane.

Mixtures with various concentrations of ethanol and water were tested with the membranes to identify if selective separation was possible. Compositions were verified by measuring specific gravity of the solutions with a specific gravity meter. This provided readings with a high degree of accuracy. The feed solution and the resulting permeate product collected was measured for each run. Ultimately it was found that for feeds of 50 and 90 mole percent there was no selectivity. For each of the three membrane materials and the two different pore sizes respectively all produced solutions having the feed composition.

While there are several possibilities for having essentially no selectivity for the membranes there are several reasons that provide understanding. The foremost is simply the pore size. While evidence was previously published suggesting that selectivity was theoretically possible with a membrane of sufficient hydrophobicity and pore sizes of up to two microns, this was not found to be the case experimentally. Likely the pores are becoming lined with ethanol and the sufficient diameter of the pore allows for both the ethanol and water to pass unhindered through the membrane.

Several recommendations were developed as an outcome of the methodological results. Firstly, to obtain further insight of the physical phenomena occurring within the pores it is necessary to further study the simulation of this system. It may be necessary to look into the

molecular interactions occurring in the pores to identify the characteristics a membrane must possess to complete this separation. From the experimental results, the membranes appeared to have pore sizes too large to selectively separate ethanol from water. This leads to the recommendation that further experiments be conducted with sufficiently hydrophobic mesoporous or microporous membranes. In addition it may be beneficial to test superhydrophobic membranes that have water contact angle measurements greater than 160 degrees.

Table of Contents

Table of Figures

Table of Tables

3 Acknowledgements

The project group would like to acknowledge the following people and groups whose contributions made this project possible.

Firstly the team would like to give many thanks to the project advisor Professor Robert W. Thompson. His valuable insight was present at every stage of the process, from initiating and conceptualizing the project to the completion of this final report. He was quick to offer guidance and suggestion whenever necessary. Without his enthusiasm and valuable time donation this project would not have been a success.

A special acknowledgement is due to several individuals who offered both their valuable time and resources. Rasesh Kotdawala offered us his previously developed MATLAB code and much of his time. He helped us tremendously with the simulation through countless emails and several teleconferences. Graduate student Brad Carleen offered valuable laboratory space throughout the projects duration but also a significant time contribution. Brad's operation of the SEM with a particularly busy schedule was much appreciated by the group. Great thanks go to Jack Ferraro, who supplied many of the laboratory materials as well as the specific gravity meter.

The group would like to thank the following organizations that made this project a reality. For supplying the membrane materials many thanks are due to GE Osmonics Laboratory. For allowing the use of a goniometer outside of normal business hours we would like to thank Triton Systems Inc.

Lastly our team would like to thank all of our family and friends, who have supported us throughout our undergraduate years in the chemical engineering department at Worcester Polytechnic Institute.

4 Introduction

Energy consumption throughout the world is on the rise. To compensate for the new demand placed on existing energy sources, primarily petroleum, alternative fuels are being heavily researched. While demand acts as a significant driving factor towards the development of new fuels there is also the drive towards making green energy. While green energy is a broad topic, encompassing many technologies the key buzzwords are renewable and sustainable. Without a doubt, the petroleum supply will ultimately be depleted, since this is a finite resource in Earth's energy infrastructure.

Ethanol, employed as a fuel for over a century, is currently receiving a significant push towards becoming a mainstream energy source. The predominant method for the production of ethanol is fermentation, distillation and dehydration. This process is commonly referred to as bioethanol production, as opposed to other methods from cellulosic ethanol and petroleum. Inevitably, the ethanol purification process has proven to be quite energy intensive.

Currently in the United States ethanol is used as a fuel additive to gasoline for several reasons. The addition of ethanol provides the combustion reaction with an oxygenate. Other reasons lie with the reason of being a "green", renewable additive, particularly when compared with the former primary gasoline additive, methyl tert-butyl ether.

The goal for this project was to identify experimentally and through modeling simulation the ability for macroporous hydrophobic membranes to separate light alcohols from water.

4.1 History of Ethanol as a Transportation Fuel Source

Ethanol has been employed as a source of fuel for nearly two centuries. Its first use as a combustible fuel began in 1826 with Samuel Morey's early work with engine development. The first internal combustion engine prototype utilized a fuel mixture of ethanol and turpentine (Hardenberg 1992). It took over 75 years before reaching the public, when in 1908 the Ford Motor Company released their first car, the Model T, with the option to run on either "ethanol or gasoline" (Kranzberg 1972). The first motor vehicles made ethanol the primary source of transportation fuel. This was most certainly the case in rural areas, where agricultural production of the fuel was best suited (Blume 2007). The transition to a gasoline-based fuel standard came several years later, caused primarily by the cheaper cost of gasoline production and the "campaign of the American Petroleum Institute" (Bernton, Kovarik and Sklar 1982).

However, recently ethanol has become a major oxygenate source in gasoline. In 1990, the Clean Air Act Amendments were enacted by Congress, which defined the US Environmental Protection Agency's responsibilities for maintaining the "nation's air quality and stratospheric ozone layer" (Congress 1990). In addition to the federal oxygenate requirement, ethanol as a gasoline additive has been caused by the phasing out of the additive methyl tert-butyl ether (MTBE). Since groundwater and soil contamination became a primary environmental concern with MTBE, ethanol demand has increased significantly (Blume 2007).

4.2 United States Transportation Energy Sector

In the United States the total energy consumption in the year 2008 was estimated by the Department of Energy to be at 99.3 quadrillion BTU. Energy consumption is further broken down into primary consumption sectors. Listed in decreasing size, the energy demand sectors

in the United States are electric power production, transportation, industrial, and residential and commercial. Shown in Figure 1 are the percentages that each of these sectors encompasses.

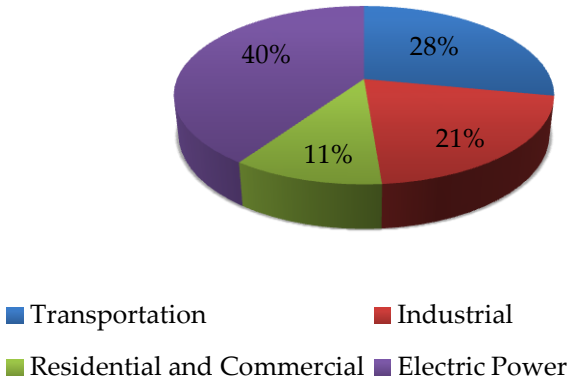

Figure 1: Energy Demand Sectors in the United States (U.S. Department of Energy 2008)

As shown in Figure 1 over a quarter of the energy consumed goes solely to the purpose of transportation. In the year 2008 the transportation market consumed 27.8 billion BTU's worth of energy in the United States. These 27.8 billion BTU's accounted for just over 28% of the total energy consumed in the United States that year. In addition to the quantity of energy consumed the source of the energy is equally important. According to the Department of Energy 95% of the 27.8 billion BTU consumed was derived from petroleum sources. The remaining energy sources are displayed in Figure 2.

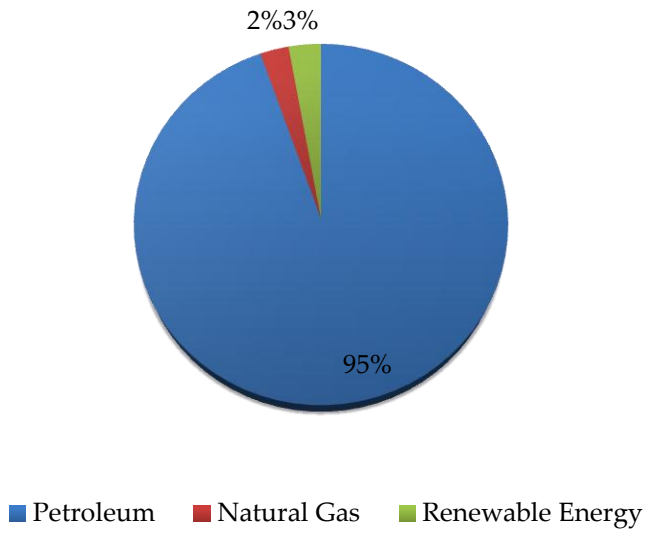

Figure 2: Transportation Energy Supply Sources (U.S. Department of Energy 2008)

Clearly the current transportation industry is dependent on the petroleum industry as its essential energy source. As shown in Figure 2, the remaining fuel sources for the transportation sector arise from natural gas and renewable energy sources, and even together these sources account for only a 5% share. Within the 3% renewable energy category is ethanol. All ethanol used in the transportation energy sector is accounted for in this category including ethanol that was blended with petroleum products.

The demand for cheap transportation fuel has increased at a near linear pace over the past 50 years.

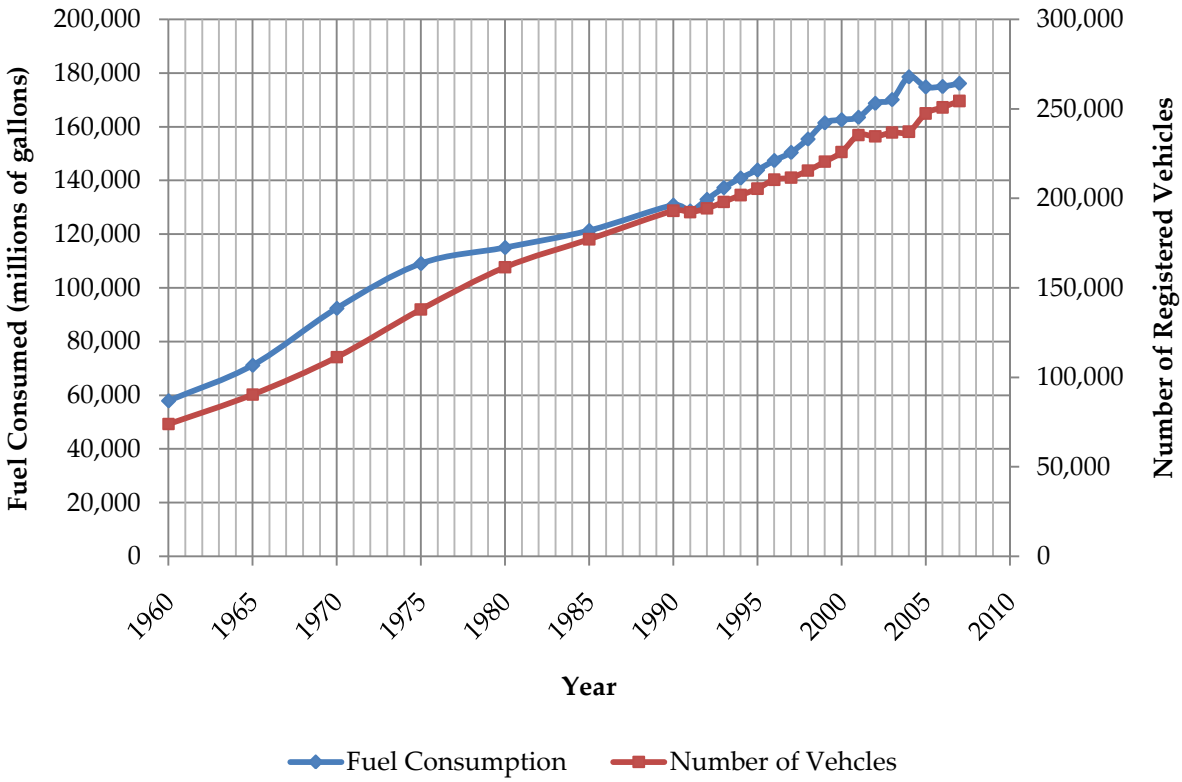

Figure 3: Fuel Consumption and Total Vehicle Registration (U.S. Department of Transportation 1960-1994) (1995-2007) (InflationData.com 2010)

As shown in Figure 3 the period from about 1970 to 1985 showed delineation from the previous exponential trend with regards to fuel consumption. Even with the fuel consumption increase receding, the growth in the total number of registered vehicles remained at a fairly constant rate. This is a direct result of the oil embargo and the push towards more fuel efficient cars. However by the 1990s when fuel was relatively cheap, the fuel consumption had again spiked. In recent years fuel consumption has become a bit unstable, likely due to the shifts in economy and gasoline prices. Ultimately, Figure 3 shows that the demand for transportation fuel has clearly increased over time in the United States.

As of present, fuel-grade ethanol is widely found in blends ranging from 10 to 85% with traditional gasoline (Blume 2007). In many countries, it is mandated that gasoline sources

contain a certain amount of ethanol. In the US and EU, most transportation vehicles can run on gasoline blended with up to 10% ethanol. There are numerous benefits and risks associated with the production and use of ethanol fuel and gasohol. Ethanol has been seen as a means of lowering dependence on foreign oil for energy sources in the US. In addition, the oxygen content in E10 gasohol burns more cleanly compared with unleaded gasoline, lowering greenhouse gases. In Table 1, the rate of the greenhouse gas emissions for different transportation fuels was considered.

Table 1: CO_2 emissions resulting from production and use of different fuels (Akinci, et al. 2008)

Fuel Type	Emission Rate
Gasoline production + combustion	67.0 kg CO_2/GJ consumed
Corn ethanol production	58.9 kg CO_2/GJ consumed
10% Corn ethanol blend + combustion	66.2 kg CO_2/GJ consumed

However, different issues begin to occur for fuel sources with higher concentrations of ethanol. Combustion in a traditional gasoline engine takes place under high pressure within a cylinder. Oxygen in the form of air enters the combustion chamber along with the gaseous fuel. The mixture is compressed and detonated through a spark. A phenomenon known as engine knocking resulted in the creation of the octane rating for motor fuels. Pure ethanol has an octane rating of 116, which allows engines to run at a higher compression ratio. This allows for more power to be obtained even though on a volume basis ethanol has approximately 2/3^{rds} the calorific content of an equal volume of gasoline (Felder and Rousseau 2005). This has caused conflicting opinions as to whether the net energy produced per unit of ethanol outweighs the energy cost per unit of production. By researching separation methods to potentially lower the

energy cost to produce ethanol, this issue could become less of a problem with strong findings to improve the current production processes.

4.3 Future Increase Considerations

In an effort to reduce American dependency on foreign oil, President George W. Bush discussed the need to produce alternative transportation fuels in his 2007 State of the Union address. He argued that a reasonable goal was to reduce the amount of oil imports by 25%. His suggestion was to "increase the supply of alternative fuels by setting a mandatory fuels standard to require 35 billion gallons of renewable and alternative fuels", which would be "nearly five times the current target" (Roberts 2007).

In June of that year, the U.S. Senate passed a modified version of a House of Representatives bill regarding this future production. The mandate encompassed renewable fuel sources, including ethanol developed from corn starch, cellulose, agricultural waste materials, and even lignin. The level of increase stated ranged from 8.5 billion gallons of renewable fuel in 2008 to 36.0 billion gallons in 2022. In addition, 21.0 billion gallons of this production was to be developed from "advanced biofuels" by 2022 (Congress 2007).

This increase has caused several major concerns for the industries involved for ethanol production. The source of the ethanol for ''advanced biofuels'' and ''cellulosic biofuels'' was not stated, except that it should not come from corn sugar or corn starch (Congress 2007). This high level of production could very likely cause worrisome effects on available agricultural land. Energy cropping would come in direct competition with food sources, since the ethanol production capabilities are estimated to exceed Conservation Reserve Program availability (Akinci, et al. 2008).

5 Background

This chapter provides the motivation for researching the developing technologies in the separation of ethanol from water. Primary focus was placed on the separation techniques. Many of the industrial scale technologies used today for the separation of ethanol and water mixtures are discussed in detail. Also of importance are some of the promising scale-up membrane technologies.

Introduced in this chapter are the background concepts of membrane separation. The common types of membranes used and some of the traditional applications of membrane separation are discussed.

5.1 Ethanol Uses

Ethanol is a simple organic compound that is one of the earliest chemicals ever produced by humanity, as early as "4000 years ago in Egypt" (McKetta 1983) and 2500 B.C. by the Mesopotamians (Cheremisinoff 1979). The primary method of production of ethanol has come from fermentation, using various strains of yeast to convert sugar compounds to alcohols. Fermentation of sugars to produce ethanol has occurred industrially for a few main purposes. The most publicly recognizable form of the compound has been seen as the psychoactive source in alcoholic beverages. However, there has been significant development for the ethanol market as a fuel source, which has motivated the majority of its contemporary production. Ethanol has also been produced as a byproduct from petrochemical refining, where ethylene from raw fossil sources is hydrolyzed using an acid catalyst (Cheremisinoff 1979). For the purpose of relevance to this MQP, more focus was placed on the separation of ethanol from sources outside of the

petrochemical refining industry, which has a separate set of considerations outside of the biomass conversion standard.

5.2 Ethanol Production

Industrial ethanol production in the form of fuel-ethanol began in 1975 in Brazil (Wheals 1999). Soon after Brazil's pioneering work, programs began developing in the United States by 1978. Since that time the primary sources for ethanol production have been sugar cane and maize. The production consists of yeast fermentation of the sugars found within a particular crop. The resulting product is distilled and further dewatered, as will be discussed in the following section.

The production of ethanol has mostly been achieved by fermentation. With recent technological advances, the process of producing ethanol is changing and new methods are being deployed to both lighten the emission of greenhouse gases and decrease the amount of energy needed.

5.2.1 Fermentation

Ethanol fermentation is an anaerobic process of producing ethanol from sugar. This process is carried out by yeast and some other forms of bacteria. The sugar is first put through glycolysis, a process which results in the splitting of a 6-C (six carbon molecule) ring sugar into two 3-C pyruvic acid molecules. These pyruvic acid molecules are then converted to acetaldehyde with the production of two carbon dioxide molecules. The final step, is converting the acetaldehyde to ethanol (Kang n.d.). In order for this conversion to take place, the reactor must be heated constantly and because of ethanol's role as a transportation fuel, a non-

transportation fuel is used. This is generally coal, which emits a high amount of carbon dioxide (Akinci, et al. 2008).

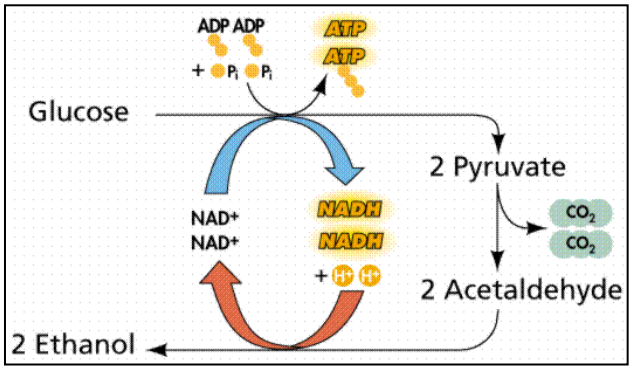

Figure 4: Fermentation Chemical Pathway (Farabee 2007)

Starches, such as corn, are also used for ethanol fermentation. The process is very similar to that for sugar, after the starch has been converted to sugar. The starch is usually converted with enzymes including diastase or amylase. The United States produced roughly nine billion gallons of ethanol from corn in 2008 (Renewable Fuels Association 2009). This shows a distinct increase from 2007 and Table 2 shows production of ethanol in the US since 2000.

Table 2: US Production of Ethanol (Renewable Fuels Association 2009)

Year	Ethanol Production (millions of gallons)
2000	1630
2001	1770
2002	2130
2003	2800
2004	3400
2005	3904
2006	4855
2007	6500
2008	9000

The amount of ethanol produced per year in the US has been increasing rapidly in the past few years, because of ethanol's role as an alternative transportation fuel. If it is to be used as an alternative to gasoline, then it must fill the void of 141.5 billion gallons needed in 2006. When looking at corn ethanol's ability to replace gasoline the limiting factor is land available for production. Using the quantity of 75 million acres of corn being harvested each year, Akinci et al. (2008) applied this amount of land to estimate the ethanol production capacity of corn. The energy content of ethanol compared to gasoline is factored in and it is estimated that using all of the corn harvested each year would only produce about eleven percent of the gasoline needed for transportation. This shows a serious problem for corn ethanol's role as an alternative fuel since that calculation was carried out with all of the corn in the US being produced for ethanol when corn accounts for 90 % of grain production in the US (U.S. Department of Agriculture 2009).

5.2.2 Cellulosic Ethanol

Cellulosic ethanol is produced from different biomass feedstocks such as agricultural plant wastes, industrial plant wastes, and crops that are grown specifically for fuel production. Feedstocks from these different sources are all made up of the same primary three components: cellulose, hemicellulose, and lignin. The cellulose and hemicellulose are then converted to simple sugars for fermentation (Greer 2005). The advantage of this process is that instead of coal being burned to heat the reactor, the lignin from the feedstock may be used as a fuel to run the process.

The advantage of this process is that the lignin from the feedstock may be burned to heat the fermentation process, which is a large portion of the energy needed. Burning the lignin for

fuel also represents a zero-net carbon emission, because the carbon dioxide released during its combustion is neglected by the carbon dioxide the plant absorbs during growth (Greer 2005).

Potential feedstock can be any type of plant remains, if the cellulose and lignin are still present. Recently, there has been some research done on converting materials from landfills to ethanol. The company, BlueFire Ethanol, Inc., has been approved for construction of a plant at a landfill in Lancaster, CA to start their production. They also have received grants for a second larger scale plant also located in Southern California. Their process uses sulfuric acid to split the lignin from the cellulose. The lignin is then recovered and used for electricity and steam. They currently can produce 70 gallons of ethanol per ton of waste. With the two plants working at capacity, over 20 million gallons of ethanol per year can be produced. They predict that a conversion of 40 million gallons per year of ethanol can be attained from landfills with construction of more plants (Biello 2008).

One of the most commonly examined feedstocks for cellulosic ethanol is switchgrass. Switchgrass poses attributes that make it a naturally good candidate for cellulosic ethanol production. One advantage of switchgrass is its deep root system which prevents erosion and promotes the soil's fertility. The plant also uses water, fertilizers, and pesticides very efficiently and therefore needs less than other plants that could potentially be grown for conversion (Greer 2005).

However, there is still a major problem of production capacity. It is not currently grown in capacity like corn so the land available for production can be taken as the amount of land in the Federal Conservation Reserve Program (CRP). Akinci et al. (2008) also performed a production capacity estimate for switchgrass. They calculated that if all 36 million acres of CRP

land (Conservation Reserve Program 2007) was used to grow switchgrass then enough ethanol would be produced to replace 6.6 % of gasoline needed for transport. Although this process produces more ethanol per area than corn does, there is still a major problem with the amount of land needed to be able to replace gasoline as the main transport fuel.

5.2.3 Algae

Ethanol production from algae is a recent breakthrough and a number of the oil industry's major companies have recently started investing in it. Ethanol can be obtained by manipulation of the algae to produce ethanol from photosynthesis. Similar to other biomass resources, the algae organisms digest in carbon dioxide and sunlight and then convert this into oxygen and biomass. Its sugars are utilized with enzymes to produce ethanol and biodiesel (Hamilton 2009).

This process takes place in large bioreactors that are partially filled with carbon dioxide enriched saltwater. The bioreactors are especially of interest because of the way that they can be run near large chemical plants. An example of this is Dow Chemical, they will have the bioreactors near the processing plant so that the oxygen the algae produce can be used to cleanly burn coal where heating is needed. In return, the carbon dioxide produced from burning the coal is then fed back to the algae to be converted into ethanol (Wald 2009).

This is an advantageous process because not only is ethanol fuel being produced, but ethanol carbon dioxide emissions are rendered neutral due to the biomass creation process. It is also advantageous because the land needed for this process is not crop land as is the case for corn and cellulosic production. However, this technology is still very new so there is still a development period to be had for algae to become a major industry competitor.

ExxonMobil has recently placed a $600 million investment in algae biofuels, joining forces with Synthetic Genomics, Inc. to "develop, test, and produce biofuels from photosynthetic algae" (ExxonMobil 2009). This appears to be a significant strategic transition as just two years earlier Exxon Mobil chief executive Rex W. Tillerson made comments that the company's stance toward renewable energy investment would not immediately change, jokingly referring to ethanol as "moonshine" (Krauss and Mouawad 2007). Exxon Mobil has also stated an additional benefit of the greater volumetric output of biofuel per acre with algae, versus other biomass sources. They have approximated, per annum, photosynthetic algae at 2000 gallons per acre, palm at 650 gallons per acre, sugar cane at 450 gallons per acre, corn at 250 gallons per acre, and soy at 50 gallons per acre (ExxonMobil 2009). This could have positive implications in future scaled-up development for this industry.

5.3 Dewatering of Ethanol

All currently implemented methods for the mass production of ethanol first result in a product of ethanol and water. Therefore, to produce ethanol of fuel grade quality the ethanol and water mixture must be separated up to 99.0 percent pure by volume, or 98.7% by weight (Vane, 2008). This single step accounts for a significant portion of the input energy for ethanol production. Hammerschlag (2006) completed a recent analysis of ethanol fuel's return on energy investment, in which it was found that the industrial processing typically required 14.0-17.0 MJ for fuel and electricity, per liter of ethanol produced.

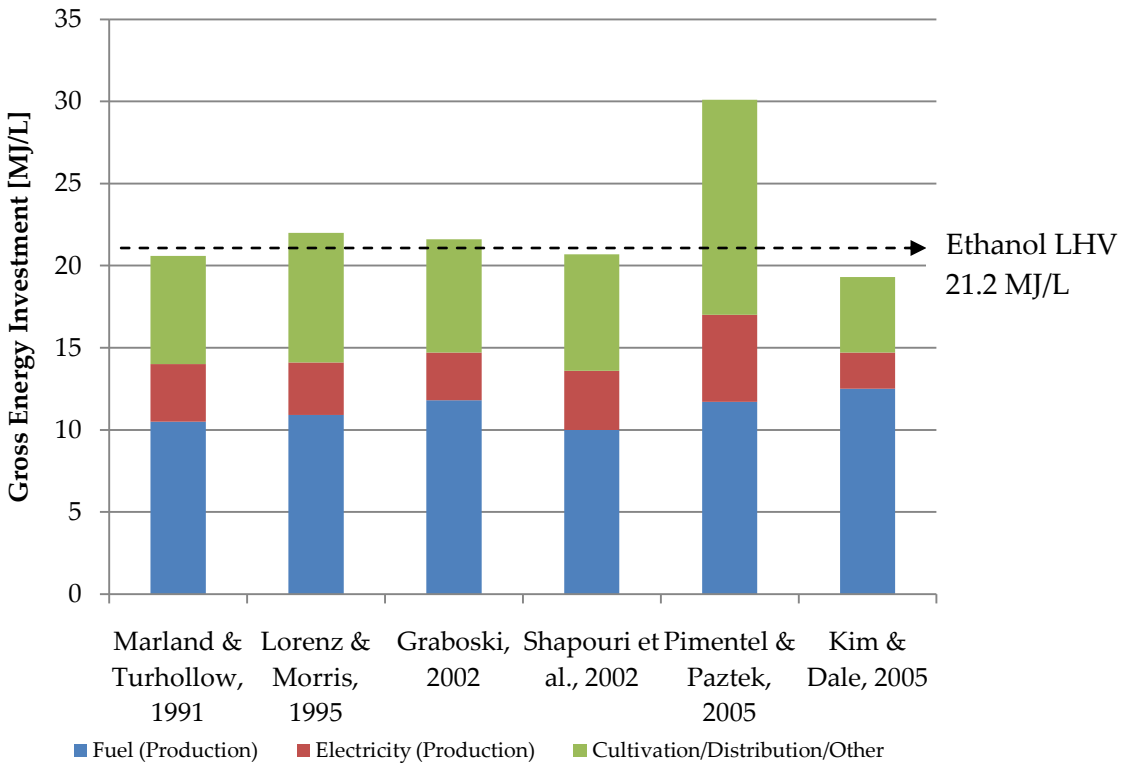

Figure 5: A review of energy input requirements for the production of transportation grade ethanol fuel

These data were gathered from a number literature sources, with various processing conditions, including wet-mill, dry-mill, mixed, and various corn/ethanol yield estimates (Marland and Turhollow 1991) (Lorenz and Morris 1995) (Graboski 2002) (Shappouri, Duffield and Wang 2002) (Pimentel and Patzek 2005) (Kim and Dale 2005). In comparison to the low heating value of ethanol at 21.2 MJ/L (Felder and Rousseau 2005), this means that around 66-80% of the overall energy output from ethanol is essentially lost in the production process, from greenhouse-gas emitting sources such as coal and natural gas.

In some ways this then becomes the drive for investigation of ethanol dewatering methods, so that ethanol energy efficiency could potentially become more reliable. The most traditional and energy efficient process used at the industrial scale today is distillation. The

technicality with distillation is that while it may be the best choice today, it is extremely energy intensive and can only produce ethanol with a volume percent of approximately 96 percent, as a result of the low boiling point azeotrope.

5.3.1 Distillation

Separation of ethanol from water producing fuel grade ethanol has long been through a chemical process known as distillation. Classic distillation involves a feed comprised of ethanol and water. As discussed in the ethanol production section the incoming feed to a distillation tower can be anywhere from 8-11% by volume (Wheals 1999), but wider range concentrations are certainly possible. Ethanol concentration can vary widely but since the largest method used to produce ethanol today is from fermentation. The majority of the ethanol refineries in operation today are fed from agriculturally produced ethanol. There are an estimated 189 ethanol refineries throughout the United States, located primarily in the Midwest where the local agriculture infrastructure is most abundant (Ethanol Renewable Fuels Association 2005-2010).

The distillation process produces two products. Classic distillation without any modifications will produce hydrous ethanol as the distillate and a bottom stream that is predominantly water. As mentioned previously, because the feed is typically 8 to 11 percent ethanol the column produces an enormous ratio of undesired water as waste product. This water mixture is known as stillage and is typically anywhere from 10 to 15 times the volume of ethanol product produced. While there are some uses for this product it requires additional advanced treatment, which increases in the energy consumption at the refinery level.

While there is a market for hydrous ethanol, which is ethanol at a purity of approximately 96% by volume, there is a greater desire for anhydrous ethanol. The biggest reason for this is the engines found in vehicles currently on the road are not built to run with hydrous ethanol (Blume 2007). Employed at the industrial scale today are several methods and operating alterations to the traditional distillation column.

Water and ethanol form a low boiling point azeotrope. At atmospheric pressure for example, pure ethanol has a boiling point of 78.4°C, while water has a boiling point of 100°C (Felder and Rousseau 2005). Therefore, in theory a mixture of water and ethanol could be heated slightly over 78.4°C and a pure ethanol vapor phase would arise. This however is not the case. As a result of the molecular interactions between ethanol and water an azeotrope forms at a boiling point of 78.2°C. Since the boiling temperature is below both water and ethanol the liquid and vapor phases become the same composition, which is approximately 96% by volume (Vane 2008).

The first method to consider is known as azeotropic distillation. Azeotropic distillation involves the addition of a third agent into the system, also known as an entrainer. The entrainer alters the azeotrope by changing the interactions of the molecules in a way such that the volatility is altered. For the binary system of water and ethanol the result is water having a lower vapor pressure allowing a purified ethanol distillate. The addition of an intermediate processing component means an additional separation process is required. This adds significant costs to the system. There is also the cost of the additional material itself that is entered into the system.

Another distillation technique used to break the azeotrope is known as pressure swing distillation. Pressure swing distillation alters the azeotrope by changing the operating pressure of the column. Figure 5 below shows a generic example of two components, A and B, that have their respective azeotrope shifted through additional pressure. The example shows that to obtain pure B from a feed concentration of F the azeotrope, D_1 must be passed. Therefore the system can be run at the lower pressure in the first column producing a product of F_2 before entering the higher pressure distillation column. The second column has the azeotrope shifted, allowing for pure product B to be obtained. This idea can be applied to the ethanol and water binary mixture to obtain a product of pure ethanol.

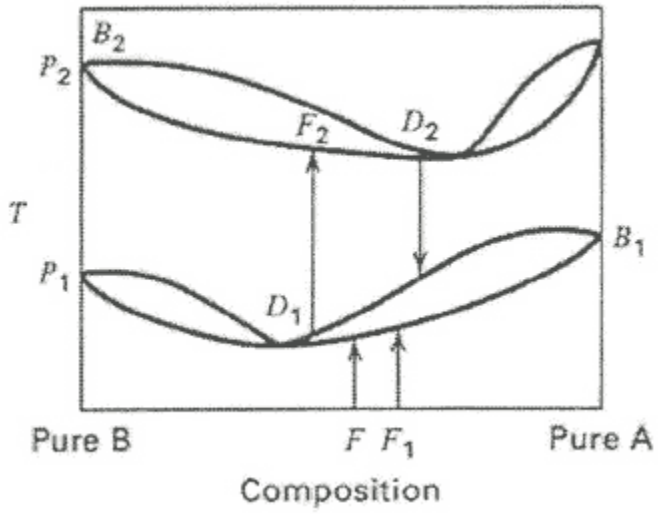

Figure 6: Generic Azeotrope Composition Change through Pressure Altering (Felder and Rousseau 2005)

Ultimately numerous methods of tweaking the classic distillation process to enable ethanol purification beyond the 96% purity composition.

5.3.1.1 Membrane Distillation

A technology related to distillation that uses membranes between trays is known as membrane distillation. The current process involves passing a vaporous feed stream through a

distillation column containing a hydrophobic, porous membrane, as seen in Figure 7: Diagram of a typical membrane distillation unit .

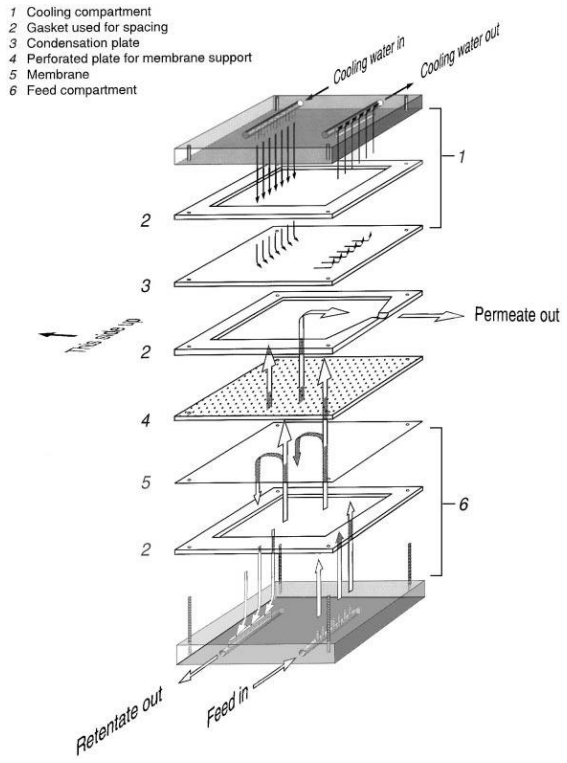

Figure 7: Diagram of a typical membrane distillation unit (Banat and Simandl 1994)

The membranes that are used can range in material, provided that hydrophobicity exists as a characteristic. Lab studies using polytetrafluoroethylene, poly(vinylidene fluoride) and polypropylene polymer membranes with a 450nm pore size investigated the mass transfer of acid/water solutions (Tomaszewska, Gryta and Moraski 2000). Lawson and Lloyd (1997) also used these membrane materials in addition to pore sizes ranging from 100-1000nm. Recently, use of MD has also been considered in seawater desalination, using 200nm polypropylene (Al-Obaidani, et al. 2008).

This process utilizes the separation factors involved with both vapor pressure differential and selective membrane transfer. Its benefits include lower operating pressure than

conventional distillation and reverse osmosis, on the order of "zero to a few hundred kPa" (Lawson and Lloyd 1997). There appears to room for more investigation into overall capital cost of this process. There are a number of additional expenses over the distillation industry standard however, including the cost of initial investment into hydrophobic membranes, the cost of replacement membranes as degradation inevitably occurs, and cost of stop/starting the unit once this replacement is necessary. In addition, this is a "thermally driven" (Lawson and Lloyd 1997)process, and since the latent heat energy requirement seen in distillation is extensive, membrane distillation might not be the most favorable solution. However, this relatively new technology is currently still on lab scale research, but it could reduce the energy consumption of current distillation practices.

5.3.1.2 Molecular Sieves

As was previously shown, the process of choice at the industrial level for the dewatering of ethanol is distillation. Since 1975 various alterations have been made to the traditional distillation process in attempts to reduce total energy consumption. Another such method widely adopted today by industry is the use of molecular sieves.

Molecular sieves are typically used in continuous processing although they require a regeneration process. The regeneration process is necessary because unlike other extraction systems, molecular sieves hold the extractant, therefore eliminating it from further processing downstream. A generic system diagram is shown in Figure 8: Generic Adsorption Process . To enable implementation into continuous processes a cyclic nature must be used (Vane 2008).

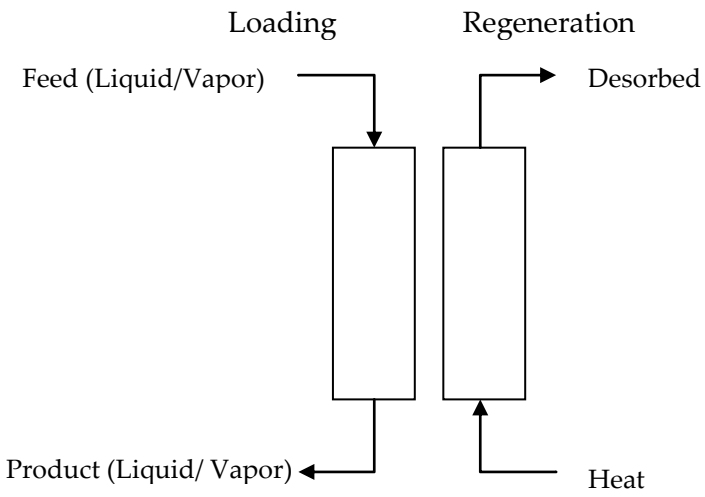

Figure 8: Generic Adsorption Process

The cyclic nature means that for a continuous distillation process there needs to be several molecular sieve units. While one is being used the other needs to be regenerated. Similar to how distillation has improved over time, so too have molecular sieves. The ideal process will incorporate many heat integration steps. The heat used to regenerate the process could come from the wastewater bottoms stream of distillation columns.

The molecular sieves themselves are typically hydrophilic zeolites with highly regular pore structures. The zeolites are often designed to be size and sorption selective. In some cases, this means that the pores are small enough for water to fit through but not the ethanol. In most other situations, the membrane has fluid-wall interactions with water that are much stronger than those with ethanol, thus making the membrane hydrophilic. This results in a high selectivity for water. It is important to note that while adsorption techniques are utilized in essentially all corn ethanol refineries, the designs and specifications are proprietary and therefore cannot be thoroughly analyzed here.

5.4 Membrane Separation

As previously discussed, energy consumption during the separation of ethanol from water is of the utmost importance. Implementing energy efficient processes is essential in moving toward expanding mass production and further industrializing the production of ethanol. The role of membrane separation technology to aid in this manner is only just becoming recognized.

Membrane separation is a broad unit operation that encompasses many different process technologies. Processes included in this branch of separation include: depth filtration (particle filtration), microfiltration, ultrafiltration, nanofiltration, reverse osmosis, electrodialysis, gas permeation, and pervaporation. Of the technologies previously listed, pervaporation is considered one of the least developed and established (Wee, Tye and Bhatia 2008).

5.4.1 Pervaporation

Pervaporation is a process that falls under the broader category of membrane separation. As its name suggests, pervaporation involves two phenomena, permeation and vaporization. In a general sense the membrane acts as a barrier through which one component has a high flux, while the other component ideally has a zero to negligible flux through the membrane. The feed side of the membrane is typically run at atmospheric (ambient) pressure, while the product side can be pulled under a vacuum to create a driving force. The resulting product that passes through the membrane is known as the permeate stream, while the retentate stream is unable to pass through (Vane 2008).

Pervaporation is a process of much current research for several reasons. One benefit it offers over a process such as distillation is its ability to get around azeotropes. Every separation technology separates by taking advantage of a particular physical property. For example, distillation uses boiling points, and molecular sieves rely on molecular size and/or sorbate/sorbent affinity. Pervaporation relies on permissibility through a particular membrane. Since pervaporation does not involve boiling points it can theoretically dehydrate an ethanol mixture to a composition distillation cannot. The vapor-liquid equilibrium that is essential for distillation does not apply since "pervaporation is almost independent of the vapor liquid equilibrium, because the transport resistance depends on the sorption equilibrium and mobility of the permeate components in the membrane (Wee, Tye and Bhatia 2008)."

With regards to energy consumption, pervaporation could benefit from a 40-60% energy reduction over competing processes (Wee, Tye and Bhatia 2008). However, energy is needed to vaporize the permeate stream. Therefore, it would be favorable to have a low concentration of the permeate stream in the feed. As was discussed previously the typical feed concentration from the fermentation unit into the distillation column of agriculturally produced ethanol varies anywhere from 7-15%, which is certainly on the lower side. The energy needed for the heat of vaporization has potential sources of being supplied by the feed or perhaps a sweeping fluid on the permeate side of the membrane. Alternatively, direct heating of the membrane is also a potential source for energy input (Feng and Huang 1997).

A pervaporation process diagram is depicted in Figure 9: Generic pervaporation process . As shown in the figure the water is the permeate stream while the organic is unable to pass through.

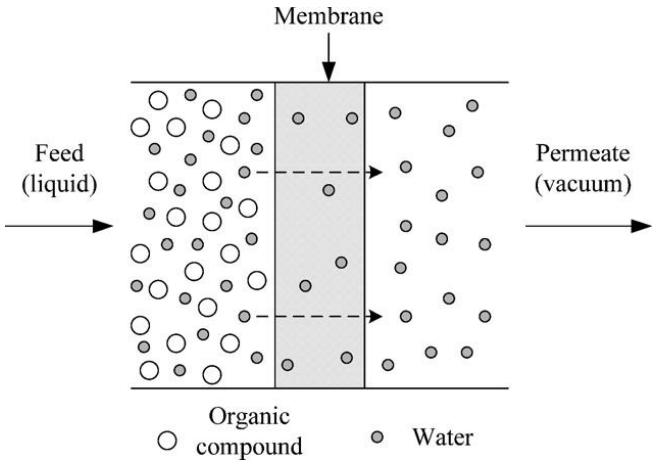

Figure 9: Generic pervaporation process (Wee, Tye and Bhatia 2008)

While Figure 8 accurately depicts a pervaporation process, it is the opposite of what was desired for this MQP. The goal for this research was to have a high organic flux through the membrane, while being impervious to water. In the most general terms flux is defined as the transfer rate divided by the transfer area. As shown in the equation below.

$$Flux = \frac{Transfer\ Rate}{Transfer\ Area}$$

To further quantify flux the following general equation in mass quantities can be used.

$$J_i = \frac{m}{St}$$

where J_i is the flux of component 'i' through the membrane, m is the mass, S is the cross sectional area, and t is the time frame. To characterize a given membrane for a separation factor two different equations are used. The following equations were used to calculate the organic selectivity for water or the organic ethanol, both using weight fractions.

$$\alpha_{EtOH} = \frac{y_0/y_w}{x_0/x_w} \qquad \alpha_{H_2O} = \frac{y_w/y_0}{x_w/x_0}$$

Where the subscripts 0 and w represent the organic and water, respectively. The x and y represent the feed and permeate. The following relationship between the selectivity should also be noted.

$$\alpha_{EtOH}\ \alpha_{H_2O} = 1$$

In addition to organic selectivity the overall selectivity of the membrane can be selected using the following equation.

$$\alpha = \left(\frac{Y}{1-Y}\right)\left(\frac{1-X}{X}\right)$$

Here the mole fraction of the more permeable component is used. The X represents the mole fraction in the feed, while Y is the mole fraction of the permeate stream.

5.4.2 Inorganic/ Ceramic Membranes

Ceramic membranes are also commonly referred to as inorganic membranes. These membranes are chiefly composed of silica, alumina, or zeolites. Ceramic membranes have a wider variety of uses than their composite or polymer competitors. The inorganic nature of these membranes makes them particularly useful for higher temperature applications as well as more aggressive solvents. Another benefit of the inorganic structure is the resistance to swelling.

Inorganic membranes and zeolites are seen throughout industry where they separate low water concentration mixtures. Their hydrophilic nature, high thermal resistance, and high chemical resistance make them especially attractive for this purpose.

5.4.3 Composite Membranes

In many pervaporation processes it is necessary to provide additional structural support. This is accomplished by using a porous support that contains greater porosity than the

desired membrane. The support structure must not hinder the permeate passage through the membrane. Therefore, the porous support structure acts solely as a base while the membrane is coated atop the structure. This structure is displayed in Figure 10.

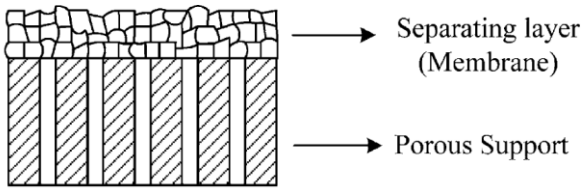

Figure 10: Membrane coating atop porous support (Wee, Tye and Bhatia 2008)

The addition of a porous support also limits the swelling of the membrane, which gives composites an advantage over traditional polymer membranes. It can be said that composite membranes "combine the superior separation performance of rigid adsorptive inorganic materials and ideal membrane forming property of organic materials" (Wee, Tye and Bhatia 2008).

5.4.4 Organic/ Polymeric Membranes

The most widely implemented membranes in industry today are polymer based. The biggest contributing factor for this is the cost. Both the materials and manufacturing process are more competitive than either ceramics or composites. Examples of commonly used polymer membranes are polyvinyldene difluoride (PVDF), polyurethane, poly(vinyl alcohol), poly(acrylic acid), and chitosan.

Polymeric membranes can be either hydrophobic or hydrophilic although the greatest use is for hydrophilic. A downside to the more hydrophilic polymer membranes is swelling. Water saturation leads to swelling which ultimately results in higher permeability but a sharp decrease in selectivity.

For the purpose of purification beyond azeotropes polymer membranes are considered to have the current advantage over composites and inorganics. Their higher flux and selectivity around azeotropic concentrations along with their associated economic benefits gives them the higher advantage.

5.5 Previous Modeling Research

There are a multitude of reasons and interests in separating ethanol from water. With regards to membrane separation, several researchers have performed detailed modeling efforts to discover the capabilities of different membrane materials and characteristics. In 2002, Giaya and Thompson investigated water-like fluids within cylindrical micropores. For simulations of pure component water, a relationship was found between fluid density, pore width, and hydrophility.

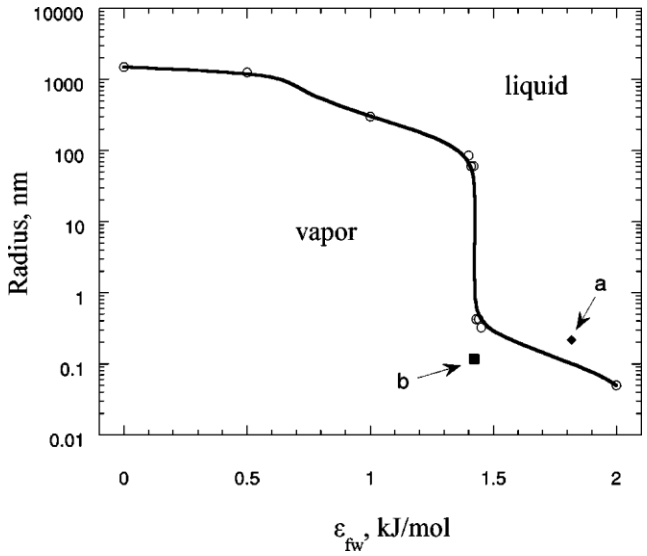

Figure 11: Pore Radius as a Function of Fluid-Wall Interaction (Giaya and Thompson 2002)

Figure 11: Pore Radius as a Function of Fluid-Wall Interaction displays the findings of this study. For membrane pores with hydrophobic properties, where fluid-wall interactions

were close to zero, water would remain in vapor phase within the pore well beyond the microporous and mesoporous range of materials (pore radius greater than 25 nanometers). Up to radial dimensions greater than 1000 nanometers, only vapor phase is predicted to occur in the pores and minimal mass transfer would be observable. This is significant since zeolites and other microporous membrane materials are often difficult to synthesize and expensive to produce.

This relationship also shows that for pure component species that have a strong fluid-wall interaction, such as an organophilic membrane with an alcohol feed, that liquid phase would be more prominent in the pores. These characteristics have prompted the direction of this project, in order to investigate macroporous membranes with hydrophobic/organophilic characteristics and the potential capability to selectively transfer light alcohols.

5.5.1 Mean Field Perturbation Theory

When using membranes to separate different molecules, there are different theories that can be used to simulate the results. One such theory that was used in this project is the mean field perturbation theory. This theory is developed to predict the molecular properties inside of the pores. The model is based on the repulsive intermolecular forces of the molecules. The model predicts the configuration energy, U_N, based on the reference system potential, U_N^0, and perturbation potential, $U_1(r)$. This is seen in the equation below (Kotdawala, Kazantzis and Thompson, An application of mean-field perturbation theory for theadsorption of polar molecules in nanoslit-pores 2005).

$$U_N = U_N^0 + \frac{N^2}{2V}\int_0^\infty 4\pi r^2 g^0(r) U_1(r) dr$$

This model will show the perturbation energy as a function of r which gives a very accurate equation of state. With this ability to accurately predict liquid properties, the model can be used to study the sorption of molecules in microporous materials. When modeling polar molecules in pores the Monte Carlo simulation is usually used as a more accurate representation. However, by adding a hydrogen-bonding term in the perturbation theory this model can now accurately predict water and other polar molecules behavior in the sorption of nanoslit-pores (R. R. Kotdawala 2005)

This project's goal of determining the feasibility of using hydrophobic macroporous membranes as a means to separate light alcohols from water was accomplished by two primary methods. These methods were developed from several overall objectives that are outlined below.

- Identify and obtain several hydrophobic organophilic membranes with various pore diameters in the macroporous range.
- Identify obtained membranes' hydrophobicity and organophilicity using basic laboratory testing including contact angle measurements.
- Develop and utilize a procedure for evaluating mass flux and ethanol selectivity from various ethanol/water mixtures.
- Reconfigure and utilize previously developed modeling software to simulate conditions similar to experimental setup.

The first three objectives were a hands-on experimental effort while the final one focused strictly on theoretical modeling. Together these objectives led to developing methods that provided sufficient data to reach the goal.

5.6 Membrane Samples

Before any experiments could take place hydrophobic membranes had to be obtained. As mentioned in the background there are many types of membranes to choose from. For their simplicity, availability, and typically low cost, polymer membranes were decided upon. Within the category of polymers alone there were many potential candidates to select from, with the ideal choice being a membrane that was impervious to water but highly organophilic. Several common materials were identified including: polytetrafluoroethylene (PTFE/Teflon), nylon, and polypropylene. As will be discussed in section 5.8.1 the equipment available in the laboratory facilitated in selecting the membranes physical dimensions. The membranes needed to be

circular with diameters of 47mm and thicknesses comparable to copy paper. Ultimately all three of the polymers previously mentioned were available from *GE Osmonics Labstore*. The membranes that were obtained are listed in the table below.

Table 3: Experimental Membrane Samples

Material	Pore Size (nm)	Thickness (µm)
PTFE/ Teflon	100	175
	220	175
	450	175
Polypropylene	100	-
	220	-
	450	-
Nylon	220	65 – 125
	450	65 – 125

Another property of tremendous consideration during the membrane selection process was pore size. For the purpose of this project macroporous membranes were desired, which are typically defined as having pore diameters larger than 50nm. As mentioned in the background, previous modeling work had suggested that pores around two microns with sufficient hydrophobicity can selectively allow organics to pass while retaining water. Therefore, with intentions of achieving high selectivity membranes with pore diameters significantly smaller than two microns were selected. For the hydrophobic materials selected (PTFE, nylon, and polypropylene) the smallest available pore diameter was 0.1µm or 100nm. As shown Table 3 several pore diameters were obtained for each of the three polymers. The objective of having several different pore diameters was to identify any influences it had on selectivity.

5.7 Contact Angle Measurements

Contact angle measurements were made to identify the hydrophobicity of the membranes. For the purpose of these experiments the contact angle is defined as the angle between the intersection of the membranes surface and the liquid droplet's interface. A goniometer and *First Ten Angstroms* software package were used to make the measurements. The instrument featured a high resolution and high zoom black and white camera to capture images and import them into the analysis software. A syringe was used to drop precise volumes of fluid on the membranes surface. Shown below in Figure 12 is an image of the goniometer and associated components.

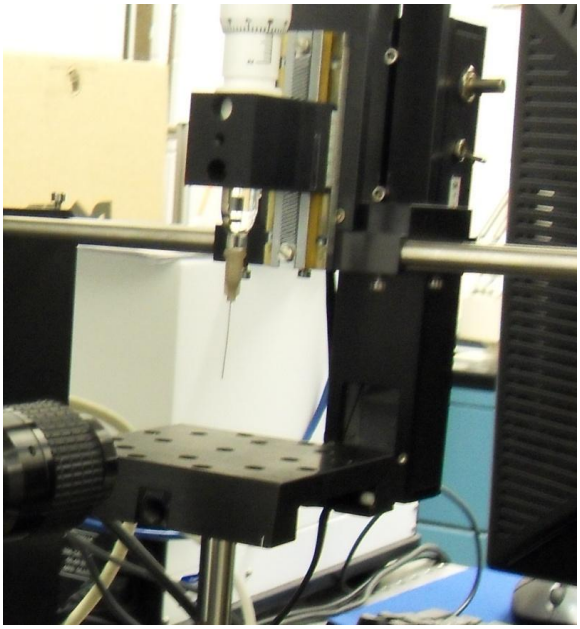

Figure 12: Goniometer, Stand, and Syringe

The sessile drop technique was used to obtain the measurements. Both DI water and anhydrous ethanol were used as the drop liquids. A picture of two 450nm Teflon membranes is shown below in Figure 13. The figure displays both the "wetting" and "beading" surface

interactions. These are examples of hydrophobic and organophilic interactions that the contact angle software can analyze.

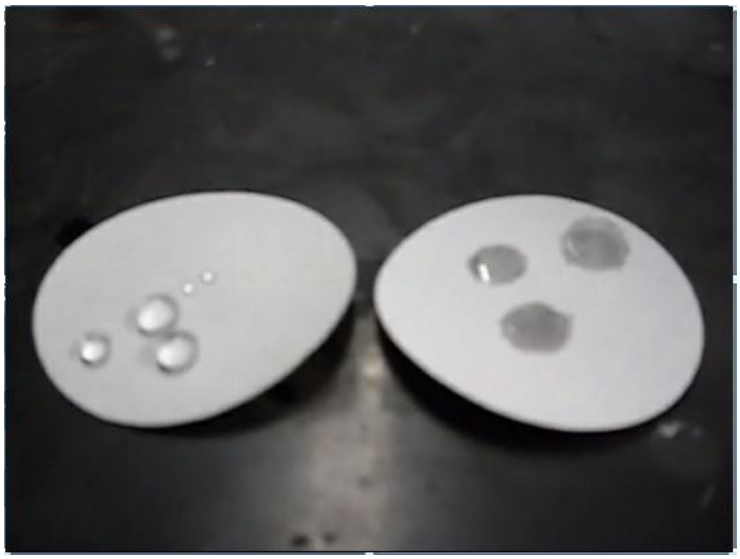

Figure 13: Different Surface Interactions – "Beading" and "Wetting"

Using a syringe a water droplet of 5µl was fed to the tip of the needle being held just above the sample. The syringe is then lowered using a manual mechanical holder, as shown in Figure 12. Once the droplet has surface contact with the membrane the syringe is then raised, resulting in the water droplet remaining on the surface of the membrane. At this point the camera is manually focused by using the computer monitor as the viewing screen. When the droplet encompasses approximately 75% of the screen a "snapshot" is taken. The highly magnified grayscale image was then analyzed by the *First Ten Angstroms* computer software to calculate the contact angle. Shown below is a sample image as it appears in the software just before being "placed" on a surface.

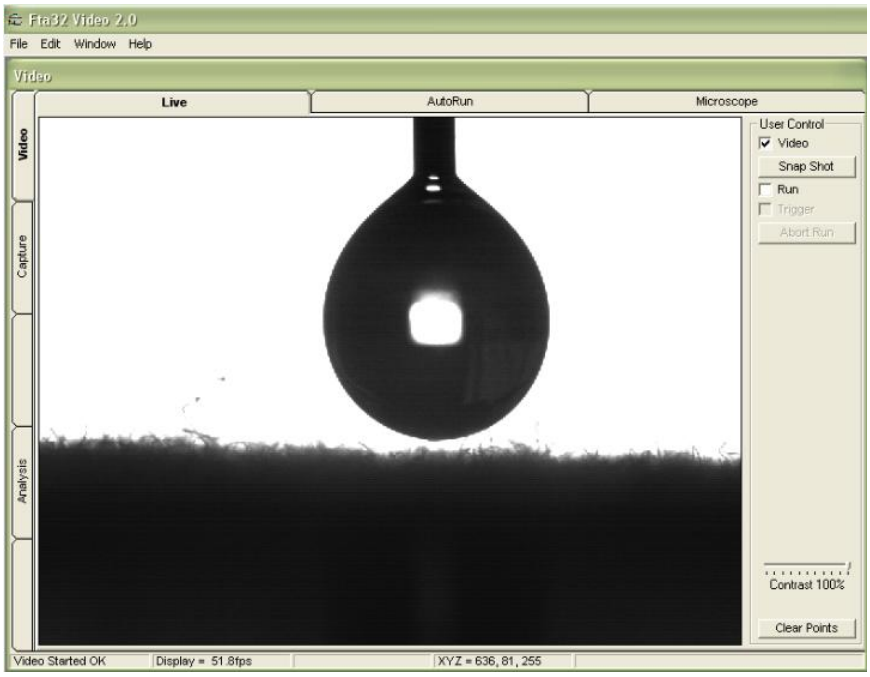

Figure 14: Water Droplet as Seen From Software

For each of the eight different types of membranes the contact angles were measured. Each type of membrane was tested on three locations over the surface and the results were averaged. Since two different liquids were studied a new membrane was used for each case to eliminate any potential interference.

5.8 Membrane Selectivity and Mass Transfer

Determining each of the sample membranes selectivity of ethanol from various ethanol and water mixture compositions was a primary objective. This was accomplished by first performing several control experiments in which pure ethanol and pure water were tested. Upon demonstrating ethanol's ability to pass freely through a membrane, pure water was then tested to ensure the membrane was impermeable to it. Flux tests were then performed with varying concentrations of ethanol. All concentrations were measured with a specific gravity meter.

5.8.1 Laboratory Setup

The physical apparatus used to hold the membranes is shown in Figure 15. The unit consisted of a flat base tray that a membrane sample rested on and then a cap and base that twisted together forming a seal around the membrane. The entire unit consisted solely of these three pieces.

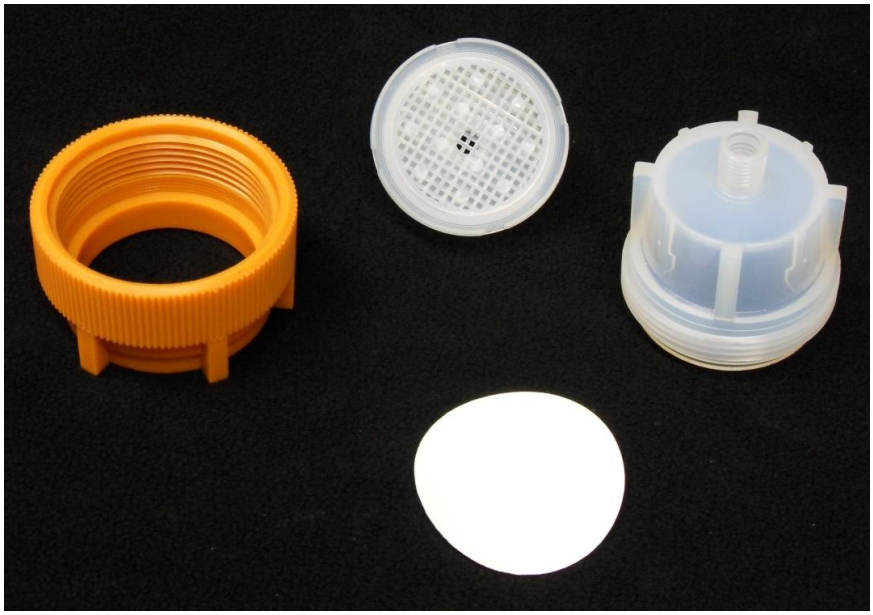

Figure 15: Membrane Holding Apparatus

The cap had a capacity of 50mL that allowed liquids to be pipetted onto the surface of the membrane. The membrane apparatus could then be held vertically allowing gravity to act as the driving force for the mixtures to pass through the pores. Upon passing through the membrane several milliliters of sample are retained beneath the membrane tray inside the base of the apparatus. To minimize buildup of permeate beneath the membrane the apparatus would be tilted whenever necessary to allow drainage into the collection beaker. Since most of the experiments required significant time to allow collection of a sufficient quantity of sample,

Erlenmeyer flasks were used. This allowed for the membrane holding device to rest atop the flask and form a crude seal as to not allow evaporation of the resulting permeate product.

5.8.2 Flux Control Experiments

Several control experiments were developed to further establish the hydrophobicity of the membranes. Anhydrous ethanol and DI water were used in two different experiments. For these experiments the membrane apparatus was fit with a membrane and then filled with 50mL of a pure component. As mentioned previously the membranes were changed for each experiment to ensure no contamination of the pure liquids that the apparatus were filled with.

5.8.3 Ethanol and Water Binary Mixtures

Several different ethanol and water mixtures were created to perform flux tests with. The compositions studied were based on mole percent and included 50/50, 90/10, and 10/90. For these experiments the specific gravity meter was used to verify the prepared mixture before testing. The resulting permeates' composition was also verified. Compositions were verified using a specific gravity meter. To use the device a sample of approximately 3mL was required. This small amount of sample allowed for testing to be completed at several different points during the collection process if desired. Since the immediate permeate was expected to be of the highest ethanol concentration the first milliliters were always tested. The initial mass flux concentration is always the data presented in the report unless otherwise noted.

5.9 SEM Imaging

As previously mentioned, the membranes utilized throughout the experimental process were manufactured with specific pore diameters. Of the eight different membranes utilized there were only three pore sizes: 100, 220, and 450nm. Since pore diameter was believed to be an

important variable pertaining to liquid- liquid separation it was desired to verify the pore diameters. A scanning electron microscope had several relevant benefits over a simple microscope. The best option for visualizing the topography of a surface is with SEM imaging. The depth of field offered by an SEM allowed for a look not only at the pore diameter but also the internal structure of the pores. SEM also allowed for samples of membranes that had been through flux tests to be tested. The purpose there was to identify if the pore structure changed as a result of being exposed to the aggressive solvent ethanol.

Samples were prepared for each of the three types of membranes (PTFE, nylon, and polypropylene) and two of the pore sizes (220 and 450nm). The additional membranes with pore diameters of 100nm were not tested as a result of having been obtained too late in the project process. Preparing the membranes for the SEM began by using a razor blade to cut the circular membranes into small squares with an area of approximately $1in^2$. These small squares were then coated with palladium as required for the SEM. During this process it was necessary to carefully cut the membranes with a sharp blade as to eliminate any chance of snagging pulling. Such physical stress would cause the pores to alter in both their shape and size.

5.10 Pore Density Simulation

The second aspect of this project was to use a previously developed model based on density functional theory with mean-field approximation to simulate the pore filling of macroscopic hydrophobic membranes (Kotdawala, Kazantzis and Thompson 2005). As discussed in the background section, previous research suggested that a membrane with sufficient hydrophobicity could selectively separate molecules of different polarities. The

properties of concern for this study included the electrostatic interactions (dipole-dipole, dipole-induced dipole, and dispersion interactions), the fluid-wall interactions, and the fluid-fluid interactions. The objective of these simulations was to identify trends in pore density as a function of pore diameter.

5.10.1 MATLAB Code

The previously developed simulation model of concern had been coded using the software package MATLAB (Kotdawala, Kazantzis and Thompson 2005). The original use of this package was studying the effects bulk pressure and density had on pore density. The code is flexible in that any binary mixture can be studied if the electrostatic, fluid-fluid, and fluid-wall interactions are known. The code also allowed manipulation of pore diameter, bulk density, and bulk pressure.

Kotdawala studied two different types of binary systems, non-polar molecules (ethane and methane) and polar molecules (methanol and water). While the code previously generated valuable data for the developer it was designed to be used specifically for the author. Without specific annotations for anyone unfamiliar with the code, learning the significance of each parameter proved difficult. The program features over 100 lines of code, abbreviated names for defining variables, and no defined units. Therefore several steps were developed in attempt to firstly reproduce previous published data from the code.

The first objective with the code was to identify the units for each of the variables. This left approximately two dozen variables. Many of these were traced back to Kotdawala's previously published work. However, several key variables were still unknown. The most

significant of which was the input variable "m," which was the bulk pressure. The remaining variables were identified through teleconferences with Kotdawala.

Shown in the table below are many of the key variables and constants that were identified within the code. The variables that are highlighted were varied, in order to determine the overall effect they had on the outputs of pore densities, Gibbs potential, and selectivity.

Table 4: Modeling Parameters of Consideration in the MATLAB code

MATLAB Variable	Definition
k	Boltzmann Constant
h	Planck's constant
N	Avogadro's number
m1	Molecule mass (comp.1)
m2	Molecule mass (comp. 2)
d	Distance between 2 wall atoms
T	Temperature
sf	Fluid Wall Interaction
esf1	**Fluid Wall Interaction (comp. 1)**
esf2	**Fluid Wall Interaction (comp. 2)**
ros	Aerial density of the solid substrate
sz	**Slit pore width**
m	**Pressure**
rob1	Bulk density (comp. 1)
rob2	Bulk density (comp. 2)
si1	Fluid-Wall Interaction
si2	Fluid-Wall Interaction
I1	Fluid-Fluid Interaction: Ionization potential (comp. 1)
I2	Fluid-Fluid Interaction: Ionization potential (comp.2)
mu1	Fluid-Fluid Interaction (comp. 1)
mu2	Fluid-Fluid Interaction (comp. 2)
rop1	**Pore density (comp. 1) (GUESS)**
rop2	**Pore density (comp. 2) (GUESS)**
s	Selectivity of comp. 2 to comp. 1

As shown in Table 4, there were a significant number of variables to account for within the code. While the majority of the variables are presented in the previous table a complete table with definition, units, values and the adjusted values range (if applicable) can be found in the appendix. Also found in the appendix is the raw unmodified code. With all of the variables defined the next objective with the code could begin.

As mentioned previously one of the objectives with the code was to reproduce previously published graphs. This would ensure a full understanding of the code. The graphs that needed to be reproduced were for a binary mixture of methanol and water. One of the graphs identified showed selectivity as a function of the bulk pressure. The other graphs showed the pore density as a function of bulk pressure and were made using bulk densities in the vapor phase and pressures less than 5kPa. Once these graphs were made the next objective could begin.

With a full understanding of the code, alterations to fit conditions similar to those in the laboratory were made. While the binary mixture studied in the laboratory was water and ethanol the binary mixture of methanol and water was expected to offer similar results. Also, many of the electrostatic and fluid interaction parameters were unknown for a binary mixture of ethanol and water. The ultimate goal for these simulations was to identify trends in pore density as a function of pore diameter. Before these simulations could begin several parameters had to be changed to represent hydrophobic membranes, mainly the esf values and sz which were identified in Table 4. This was accomplished primarily through guess and check methods but also with the input of the code developer Rasesh Kotdawala.

6 Results and Discussion

This chapter presents the results obtained from the laboratory and simulation portions of the methodology. All discussion and associated analysis represents the best understanding of the complex phenomena associated with the findings.

6.1 Hydrophobicity

Before any separation experiments could be performed the membranes were evaluated for both their hydrophobicity and organophilicity. These experiments were performed by the means of contact angle measurements and pure component flux tests.

6.1.1 Contact Angle Measurements

Contact angles were measured as described in the methodology. Shown below are tabulated averages for the water contact angles measured for each of the different membranes.

Table 5: Average Water Contact Angles

Sample	Average
Teflon	
100nm	146
220nm	145
450nm	146
Nylon	
220nm	145
450nm	144
Polypropylene	
100nm	144
220nm	144
450nm	146

As shown in the table each of the eight membranes had significant hydrophobic characteristics. While there is no exact cutoff point, a material possessing a contact angle of over

160 degrees is considered to be superhydrophobic, which suggests that these polymers can be classified as highly hydrophobic. These data also show that the water contact angle is not affected by the pore diameter. The range of diameters from 100 to 450nm offers a wide degree of variation in the macroporous region. During testing it was also noted that the water droplets were stable for 15 minutes after testing. This result suggested that the membranes were impervious to water, but further testing was performed to verify this assumption. This will be discussed in more detail in the following section dealing with control flux testing.

Noticeably absent from Table 5 are the contact angle values for pure component ethanol. This is because the testing resulted in a contact angle of zero for all membrane species. Immediately upon contact with the membrane surface the ethanol droplet wicks into the pores. Since wicking occurred with each of the membranes the data suggested that the membranes are organophilic. Once again this theory was further tested and the results can be found in the control flux testing section.

6.1.2 Control Flux Testing

As shown and discussed in the previous contact angle measurement section the three polymer membranes are highly hydrophobic and organophilic. To further demonstrate these properties flux testing was performed with pure component ethanol and water. For these tests anhydrous ethanol and de-ionized water were used. Membranes were not reused to eliminate cross contamination and to ensure the membranes were always operating at what was considered to be new condition. Shown below are the tabulated results for the flux of pure component ethanol.

Table 6: Pure Component Ethanol Flux Data

Sample	Average Flux ($g/m^2/s$)
Teflon	
100nm	0.41
220nm	0.89
450nm	1.09
Nylon	
220nm	0.32
450nm	2.05
Polypropylene	
100nm	0.41
220nm	0.55
450nm	0.72

As expected the larger pore sizes allowed for a larger flux, as there was more open area for molecules to move through. However there were several experimental observations to consider with respect to these flux values. For the first few experiments the flux values were obtained by allowing the complete transfer of a known input volume. However, since the transfer of even a small volume was found to take hours in many cases the method was adjusted. Since anhydrous ethanol is so volatile significant error was introduced by allowing the flux to occur for several hours. Even after covering the apparatus vaporization of the ethanol was a concern. Therefore the experiments were adjusted to run for a set period of 15 minutes after which the sample that transferred would be massed.

Another reason for adjusting the experiments was the concern of introducing error by allowing the membranes to soak for a prolonged duration in the anhydrous ethanol. This became a concern after observing that flux changed with time. The initial few milliliters represented the highest rates of flux. The reasoning behind this was twofold. As just mentioned,

it was expected that membrane soaking was occurring. Another reason was as the level and volume of liquid atop the membrane decreased the gravity driving force was reduced. Therefore, to eliminate these concerns the experiments moved to a set time period of 15 minutes.

Pure water flux tests were performed in a similar manner to the ethanol. As expected, flux tests showed the polymer membranes were impervious to pure component water. For these experiments 50mL of water was placed in the membrane holding apparatus, atop the membranes, just as was done with the ethanol flux tests. However, since zero transfer occurred over a one hour time period the tests were allowed to continue indefinitely. After having observed that the pure water was stable atop the membranes surface days later, it was concluded that the membranes were indeed impervious to pure water. Ultimately, de-ionized water does not transfer through the membranes.

It was hypothesized that the pure component ethanol flux values shown in Table 6 represented the highest possible flux for these membranes. The reasoning here was based off the observations about the water contact angles. Pure water was seen to have beaded up on the membrane surface and remained stable for the duration of experimental testing. Therefore it was believed that any increase in the concentration of water would reduce mass transfer. To prove this theory binary mixture flux testing was performed. These experimental results and further explanation are provided in subsequent sections.

6.2 Binary Mixture Selectivity Testing

After completing pure component control flux testing the next step was binary mixture selectivity testing. The objective here was to identify if selective transfer was possible. For the basis of this project it was hypothesized that macroporous hydrophobic membranes would selectively separate ethanol from ethanol/water mixtures. To perform these tests several binary compositions of ethanol and water were selected. On a molar basis the mixtures utilized in the laboratory were 10, 50 and 90 percent ethanol, with the remaining contents being de-ionized water. Using such a wide range of compositions had the added benefit of being able to check if the selectivity was a function of the bulk composition. While it may seem that three compositions may not be enough to identify such trends it was decided that additional mixtures would be tested if favorable results were obtained.

Shown below in Table 7 are the average selectivity for each of the membrane samples.

Table 7: Average Ethanol Selectivity Data

Material	50/50 EtOH Avg. Selectivity	90/10 EtOH Avg. Selectivity
Teflon		
100nm	**0.98**	**1.06**
220nm	**0.98**	**0.98**
450nm	**0.92**	**1.05**
Nylon		
220nm	**1.01**	**1.03**
450nm	**1.05**	**0.95**
Polypropylene		
100nm	**0.98**	**1.00**
220nm	**0.96**	**1.04**
450nm	**1.01**	**0.98**

As shown in Table 7 the selectivity for all tests were very close to 1.0. This means that no selective transfer of ethanol occurred and that the bulk phase composition passed freely through the membrane pores unchanged. As shown by the table the values are not perfectly one in every case. This is easily explained by error in experimentation rather than a result of selective transfer. The biggest source of error was the result of ethanol vaporization, which quickly changed compositions especially when dealing with small volumes.

These binary selectivity tests were performed in a similar way to the pure component flux tests. A volume of 50mL of sample mixture was placed in the apparatus atop the membranes. Both the initial and final compositions were measured using specific density. For reference the conversion chart is provided in the appendix.

It is worth noting that flux values are not reported for these binary mixture tests. The reasoning here is that they do not provide any additional valuable insight into the membrane transfer. However it should be noted that as hypothesized in the pure component flux section, the rate of flux decreases with increasing concentration of water in a binary mixture.

As was previously mentioned, three different compositions were tested while Table 7 only presents data for the 50/50 and 90/10 ethanol mixtures. The reason for this is that the 10% ethanol mixture exhibited zero flux for all membrane samples. This was verified by sealing the apparatus and allowing it to continue running for extended time. By remaining stable for more than 24 hours, it was concluded that the membrane did not allow transfer of the 10% ethanol mixture.

While all separations performed in this experimental section had a driving force of only gravity, it was attempted to place a pressure gradient across the membrane. This was performed with the binary mixture of 10% ethanol, which did not exhibit flux. It was found that a pressure gradient of less than one atmosphere gauge pressure caused complete and nearly instantaneous flux. While this does not provide insight into the selectivity this simple test further demonstrated that the macroporous membranes would be unable to be implemented at the industrial scale where the most likely implementation would be in a system with a high pressure gradient across the membranes.

6.2.1 SEM Imaging

For the purpose of identifying the pore distribution on each of the membranes an SEM was used. Several different zoom levels were tried, 2000X, 6000X, and 7000X. Ideally images would have been taken that were several microns across, perhaps two to three microns. However, as a result of coating the membranes with palladium they become highly charged and can burn at higher magnifications.

There were several observations from the SEM which stand out. Firstly is that the pores are not actually cylindrical. They are instead better described as a matrix of networked channels. This allows for molecules to pass to adjacent channels during the diffusion process. Shown below is a sample image from the SEM that clearly shows the networked channel structure of the membrane.

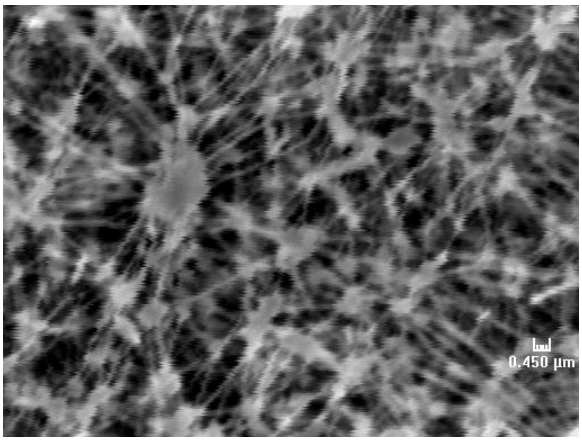

Figure 16: Dry Teflon 450nm - 6000X

Another important observation was that the pore size distribution had a large degree of variation. In many cases it was possible to identify pores with sizes of approximately 2 microns while the labeled retail description was 0.45 microns. From a qualitative perspective these larger pores allowed for higher rates of flux. Quantitatively it is impossible to say to what degree these pores played in the selectivity tests performed. While unrelated to these membranes, pore diameter is a critical parameter in many cases, zeolites being the primary example. As discussed in the background, zeolites structure in many cases dictates the separation ability.

Another goal that was made when using the SEM was to compare membranes that just taken out of packaging against those that were soaked for 30 minutes in a mixture of 50/50 ethanol and water. The soaked membranes were allowed to air dry before being coated with palladium. While the SEM images can be found in the appendix the findings for the testing were inconclusive. In many cases the soaked membranes did appear degraded but the extent and validity of this claim is difficult to support.

6.3 Binary Mixture Simulation

Extensive runs were performed with the MATLAB code previously developed by Rasesh Kotdawala. Shown in Table 8 below are the parameters and respective ranges that were adjusted for the simulations.

Table 8: Simulation Parameters Modified

Parameter	Definition	Range
esf1	Fluid Wall Interaction (comp. 1)	0 – 65.32
esf2	Fluid Wall Interaction (comp. 2)	74.22 - 100
sz	Slit pore width	18 - 4500
m	Pressure	0.006 - 4000
rop1	Pore density (comp. 1) (GUESS)	1e20 - 5e28
rop2	Pore density (comp. 2) (GUESS)	1e20 - 5e28

As mentioned previously there were several objectives for these simulations. Firstly, it was desired to reproduce previously simulated results by the code's author Kotdawala. The idea was that reproducing previous work would demonstrate understanding of the code. Since the MATLAB code solves a system of nonlinear equations there are many times when the program will output unreal answers, such as negative or unreasonable pore densities. To produce real answers it was essential to monitor the associated Gibbs free potential with each simulation.

6.3.1 Recreating Similar Gibbs Energy and Selectivity Studies

The laws of thermodynamics state that "The lowest Gibbs free energy is the stable state," (Gaskell 2008) therefore it was critical to monitor the simulated results Gibbs free energy. Shown below by Figure 17 are the MATLAB simulation outputs for Gibbs energy from this project, in a system similar to Kotdawala's previous work.

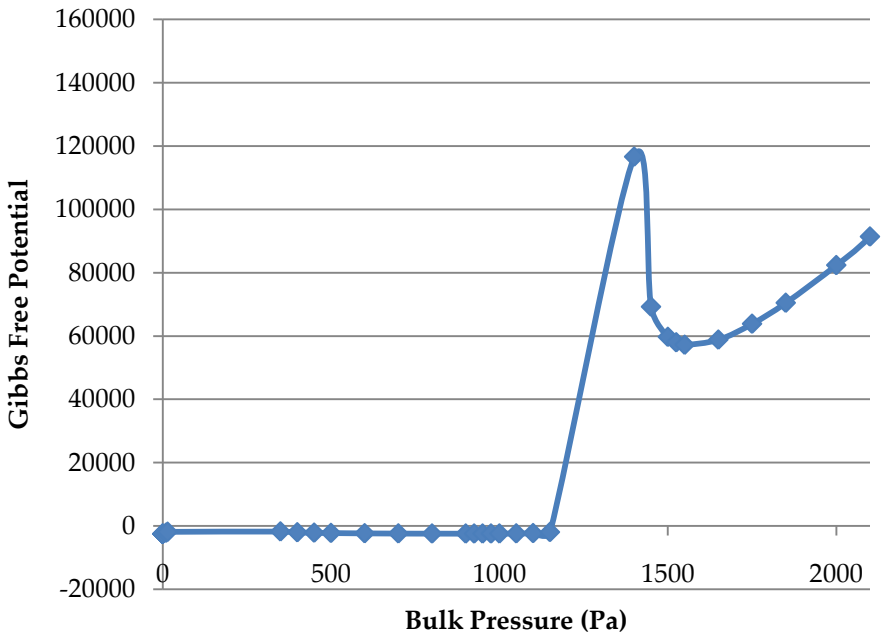

Figure 17: Gibbs Free Potential – 18 Angstrom Hydrophilic Pores

It should first be noted that the units of Gibbs free potential from the simulation outputs are unknown. The significance of this figure comes from the general trends of the data. In this figure, it is apparent where a phase shift is occurring in the pores. Before the capillary jump, the Gibbs free potential is minimal, at negative values close to zero. This represents a very stable vapor density phase in the pores. At the point where condensation occurs, an asymptote is visibly apparent. This high value of Gibbs energy marks the unsteady equilibrium point where capillary condensation occurs. After this point the Gibbs potential decreases, but does not return to negative values, and it is greater in magnitude than the vapor density range. This is expected as previously work from Giaya suggests, shown by Figure 18 below.

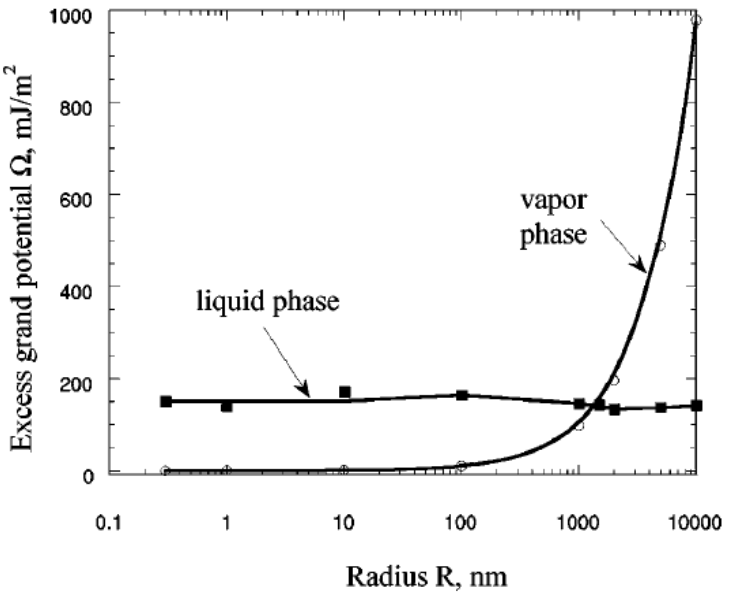

Figure 18: Excess Grand Potential vs. Pore Radius (Giaya and Thompson 2002)

The figure above demonstrates that the stable phase is that which is lowest in energy. Upon approaching capillary condensation the vapor phase becomes unstable and therefore increases in grand potential energy. Upon crossing the liquid line the stable phase becomes the liquid phase.

Membrane selectivity can be simulated as well with the MATLAB code. Shown below is a sample MATLAB simulation output from this project, again for a system similar to what Kotdawala studied.

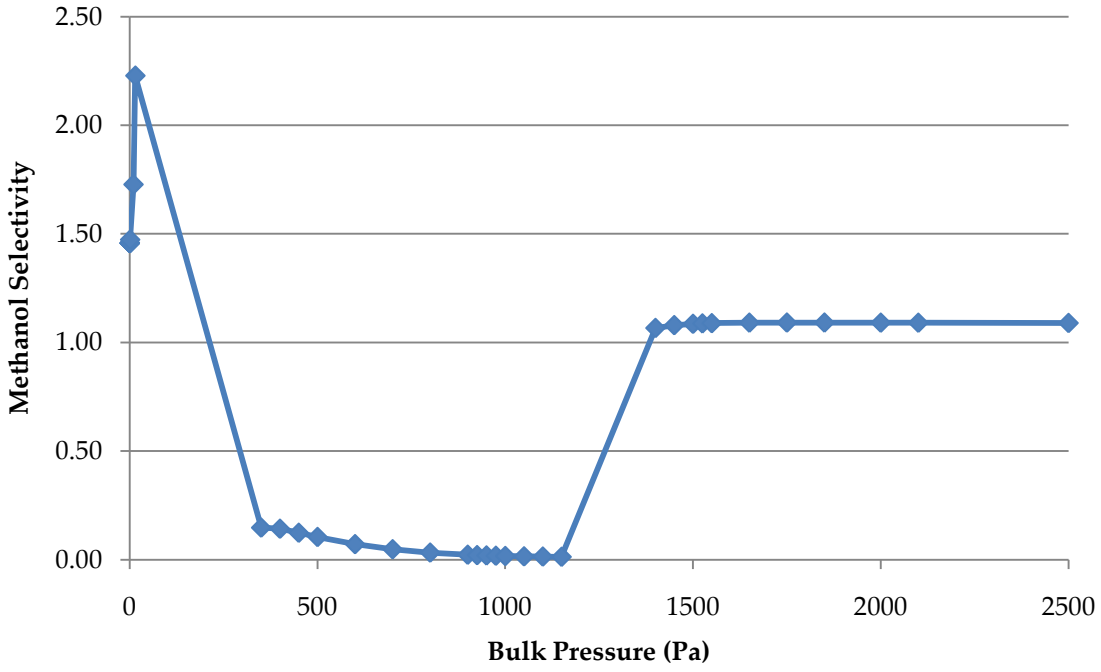

Figure 19: Hydrophilic 1.8nm Pore Selectivity

The first observation of the selectivity figure above is the shape. Up to the point of approximately 300Pa the selectivity appears to be jumping around. This is partly attributed to the extremely low bulk pressure. In this range of pressure the selectivity is highly sensitive since there is such low vapor density in the pores. Upon a more stable pressure the selectivity levels out to where the pores favor water vapor. Upon capillary condensation the selectivity essentially reaches 1. Therefore the bulk phase of 50/50 – methanol/water is allowed to pass through the pores unrestricted.

6.3.2 Adjusting Fluid-Wall Interactions

Upon demonstrating simulation results with trends similar to those of previous work the second objective began. The second objective focused on adjusting the fluid wall interactions parameters to represent pores that are both hydrophobic and organophilic. The reasoning for these modifications was to simulate membranes with properties similar to those

used in the laboratory. Within the MATLAB code the fluid wall interaction parameters were defined as the constants "esf1" and "esf2." Since it is unfeasible to know the exact values for fluid wall interactions that any particular membrane would have with any particular molecular species there was significant guess and check required. Also of use were best estimation methods and input from the developer of the code, R. Kotdawala.

Shown in Figure 20 below is the result of adjusting only the fluid wall interaction parameters. Two different conditions are shown. The first represents a membrane similar to those studied by Kotdawala while the second condition demonstrates maximum hydrophobicity and further organophilicity.

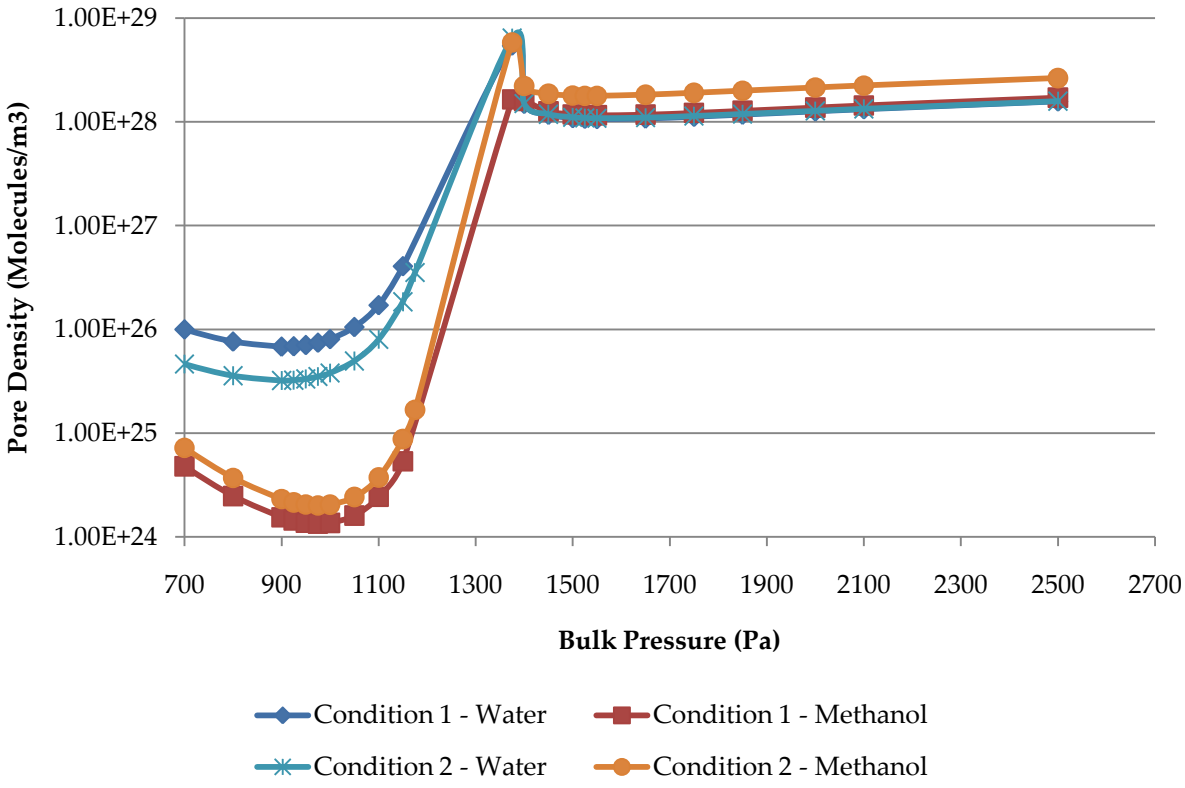

Figure 20: 18 Angstrom Pores, Condition 1 – (Hydrophilic, Organophilic), Condition 2 – (Hydrophobic, Increased Organophilicity)

As shown by the figure the fluid wall interaction parameters have an insignificant affect on the pore density. Both of the conditions show that capillary condensation occurs at the same bulk pressure. Shown below are the run parameters used for the previous figure.

Table 9: Run Parameters for Figure 19

	Condition 1	Condition 2
esf1	65.32	0
esf2	74.22	100

Another observation is that the selectivity is essentially the same for both cases. Furthermore, this simulation shows that increasing the hydrophobicity has essentially no effect in changing the fundamental behavior of the system. It was expected that a perfectly hydrophobic pore would eliminate or significantly reduce the pore density of the water and that by increasing the organophilicity, the methanol would be preferentially condensed within the pores. However, upon simulation it was found that this was not the case in the vapor phase and only slightly true after capillary condensation.

6.3.3 Adjusting Pore Diameter

After identifying the simulation effects of adjusting the fluid-wall interactions it was necessary to adjust the pore diameter. Shown in the figure below are the results of running two sets of very different conditions. The two membranes compared in the figure are a highly hydrophilic microporous membrane similar to those in Kotdawala's work (18 nm) and highly hydrophobic macroporous membrane are similar to those used in the laboratory experiments (450 nm). In the figure "Condition 1" is the same as that found in Figure 20 and "Condition 2" is also the same as Figure 20 except the pore size was increased.

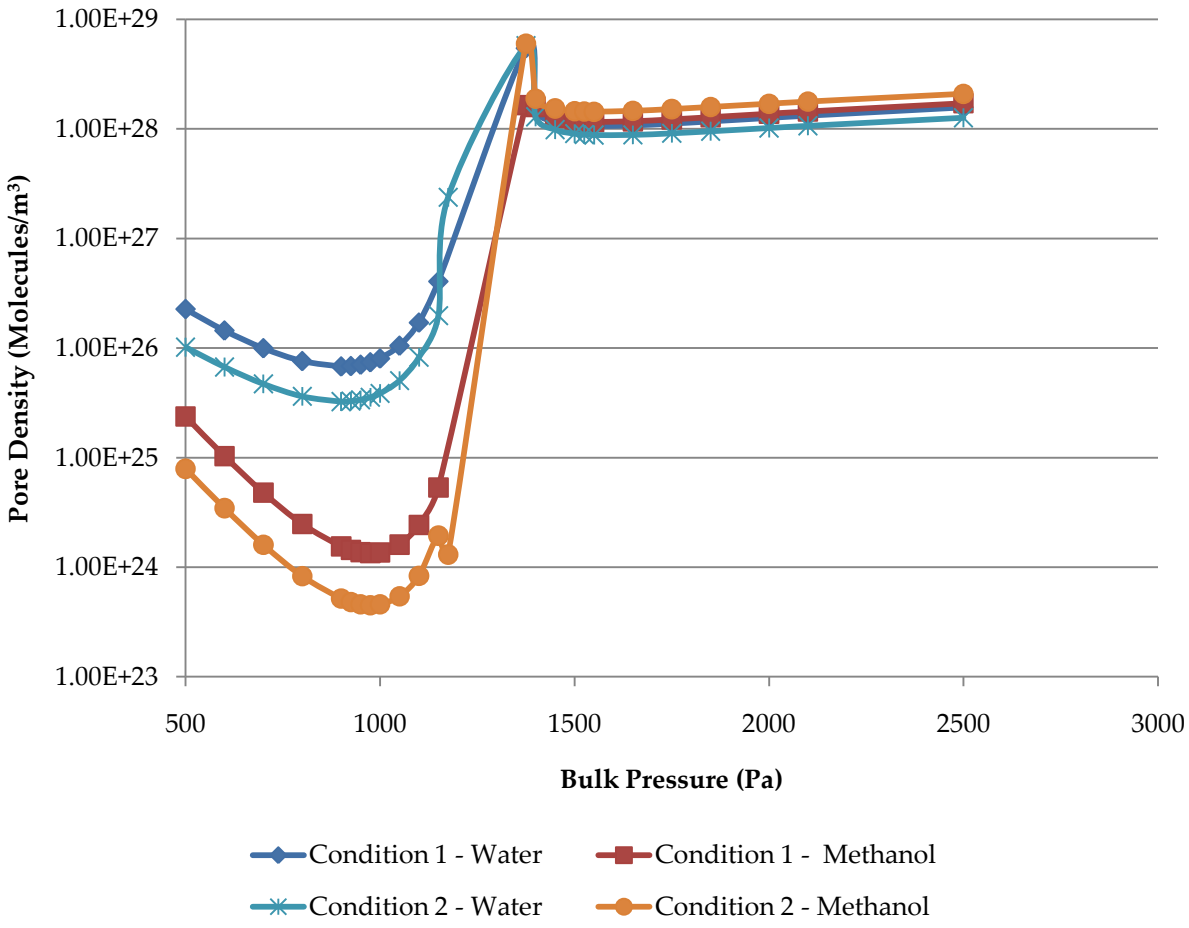

Figure 21: Condition 1 - Microporous/Hydrophilic; Condition 2 - Macroporous/Hydrophobic/Organophilc

The biggest observation here is that the input parameters minimally modify the simulation results. For a microporous/ hydrophilic pore it was expected that upon capillary condensation water would be fully condensed within the pores with the organic methanol at a lower pore density. This would demonstrate to be water selective. As shown in the above figure this trend is simulated correctly. Conversely it was expected that the macroporous/hydrophobic simulation would show capillary condensation to have equal molar concentrations to the bulk phase. Even if it did not show that the concentrations were equal, it could have also made sense to see the pore density favor methanol over water. However this was not found to be true. As

shown in the figure the graphs share similar curves when they have tremendously different input parameters. The differences in inputs are shown in the table below, where "k" represents the Boltzmann constant.

Table 10: Input Differences

	Condition 1	Condition 2
esf1	65.32*k	0.0*k
esf2	74.22*k	100*k
sz	1.8 nm	450 nm

From the inputs shown in the table above, the simulated results certainly did not agree with what was expected. This was an unfortunate finding that suggested either the MATLAB code was unable to simulate the desired system or something was wrong beyond the project groups' knowledge of the code.

One main objective with the simulations was to show the relationship between pore density and pore diameter. Therefore several runs were performed in both the macroporous and microporous range. Shown below in Table 11 are the water pore densities for various input pressures and pore diameters.

Table 11: Water Pore Density - Hydrophobic Pores

m	1.8nm	100nm	220nm	450nm
0.006	3.00E+22	3.00E+22	3.00E+22	3.00E+22
0.007	3.50E+22	3.50E+22	3.50E+22	3.50E+22
0.008	4.00E+22	4.00E+22	4.00E+22	4.00E+22
0.009	4.50E+22	4.50E+22	4.50E+22	4.50E+22
0.01	5.00E+22	5.00E+22	5.00E+22	5.00E+22
1	5.00E+24	5.00E+24	5.00E+24	5.00E+24
10	4.99E+25	4.99E+25	4.99E+25	4.99E+25
100	4.68E+26	4.68E+26	4.68E+26	4.68E+26
500	1.02E+26	1.02E+26	1.02E+26	1.02E+26
900	3.25E+25	3.25E+25	3.25E+25	3.25E+25
1000	3.85E+25	3.85E+25	3.85E+25	3.85E+25
1100	8.22E+25	8.22E+25	8.22E+25	8.22E+25
1200	2.55E+27	2.55E+27	2.55E+27	2.55E+27
1400	1.29E+28	1.29E+28	1.29E+28	1.29E+28
1500	8.87E+27	8.87E+27	8.87E+27	8.87E+27
2000	1.02E+28	1.02E+28	1.02E+28	1.02E+28

From Table 11 it is clear that pore diameter has no affect on the pore density within the MATLAB simulation code. This table was highly unexpected as the physical differences in the inputs are tremendous and even slight differences should have occurred. The pressure range used for these results encompassed the capillary condensation jump, which means that pore diameter had no affect at all. After obtaining these data it was evident that identifying the effect pore diameter had on capillary condensation was not possible. While these are the reported results from the simulation they are improbable in reality.

Another possible reasoning for Table 11 showing no change in pore density relates back to Figure 11 found in the Background Section. For example, starting at point "a" on Figure 11 and increasing the pore diameter shows that the liquid pore density remains the stable phase.

However, the presence of alcohol might affect the vapor/liquid coexistence curve for pure water shown by Figure 11, appearing to create a more hydrophilic environment in the pores. While not provided here, further simulations with pore radius less than the smallest used above (1.8 nm) could show that the pore density could shift.

6.4 Final Conclusions

The separation of binary mixtures of ethanol and water using hydrophobic macroporous membranes is not a feasible technique. None of the three materials of nylon, polypropylene, or Teflon provided favorable separation. Control experiments showed that the membranes were highly hydrophobic and organophilic. However, upon testing binary mixtures it was shown that the selectivity achieved was essentially one, meaning that the bulk composition remained unchanged. It was also shown that increasing pore diameter allowed for higher rates of flux but had no impact on selective transport. These experimental findings suggest that the hydrogen bonding interactions between the water and ethanol molecules appear to be stronger than the hydrophobic wall effects of the membrane pores.

Several observations and conclusions were developed for the simulation aspect of the project as shown below:

- It is important to understand that the simulations conducted during this project did not outright reproduce the simulations Kotdawala had developed in 2005, using the same input variables. This single aspect of the results has taken a significant amount of time to investigate. Without seeing the same results under the same initial conditions, this has put validity of the simulations conducted during this project into question. Nevertheless, analysis of what was found did prove to show some favorable trends.
- In each scenario, there was a bulk pressure point where capillary condensation appeared to occur. This was noticeable since the pore densities "jumped" to values greater than

bulk density, as Kotdawala himself had noted. This was also seen in the jump of Gibbs potential values at the same bulk pressure.

    - However, all simulations produced this jump at around the same bulk pressure point, independent of fluid-wall interactions or pore size.

- Where the apparent capillary condensation occurred, it was witnessed that the alcohol-to-water selectivity was about 1.0. This was also seen in the experimental lab results.

6.5 Recommendations

Several recommendations were developed upon conclusion of the project. These recommendations are built upon the results obtained through both the laboratory and simulation portion of the project. Together they provide a future direction for the study of macroporous membrane technology as well as general alcohol and water separation.

- **Different binary mixtures:** While the focus of this project was light alcohol purification these membrane materials have properties that could be applicable to other separations. As shown by the contact angle measurements and the pure component water flux tests, the relatively inexpensive polymers nylon, polypropylene, and Teflon are impervious to water. Mixtures of polar and non-polar components could take advantage of these properties with selectivity that could be favorable. There are many ways to separate oils from water but membrane separation could be a viable option in some situations.

- **Superhydrophobic, mesoporous/microporous:** While the highly hydrophobic macroporous polymers were unable to provide selective transport, different physical properties could produce favorable selectivity. Increasing the hydrophobicity to obtain contact angles higher than 150 or even 160 degrees could aid in the separation. Also, as has been shown the pore diameter is a key parameter for separation. While it is difficult to get polymers with pore sizes on the meso- or microporous scale could aid in favorable results.

- **Simulation:** The simulations performed with the modified code obtained from Rasesh Kotdawala did not produce expected results. In order to confidently run the simulations the best recommendation would be to redevelop the MATLAB code from the original equations of state. Fully documenting all work is essential to allow future users the ability to modify and build upon previous work.

7 References

AEA Technology PLC and C.A. Lewis. *Fuel & energy production emission factors.* 1997. http://www.inrets.fr/infos/cost319/MEETdeliverable20.pdf (accessed 2009).

Akinci, Berk, Paul G. Kassebaum, Jonathan V. Fitch, and Robert W. Thompson. "The role of bio-fuels in satisfying US transportation fuel demands." *Energy Policy*, 2008: 3485-3491.

Al-Obaidani, Sulaiman, Efrem Curcio, Francesca Macedonio, Gianluca Di Profio, Hilal Al-Hinai, and Enrico Drioli. "Potential of membrane distillation in seawater desalination: Thermal efficiency, sensitivity study and cost estimation." *Journal of Membrane Science* (Elsevier) 323, no. 1 (2008): 85-98.

Banat, Fawzi A., and Jana Simandl. "Theoretical and experimental study in membrane distillation." *Desalination* 95, no. 1 (March 1994): 39-52.

Bernton, Hal, William Kovarik, and Scott Sklar. *The Forbidden Fuel: Power Alcohol in the Twentieth Century.* New York: Boyd Griffin, 1982.

Biello, D. "Trash-Based Biofuels: From Landfill to Full Tank of Gas." *Scientific American Web site.* February 12, 2008. http://www.scientificamerican.com/article.cfm?id=trash-based-biofuels#comments (accessed September 29, 2009).

Blume, David. *Alcohol can be a Gas.* Sanat Cruz, California: International Institute for Ecological Agriculture, 2007.

Cheremisinoff, Nicholas P. *Gasohol for Energy Production.* Ann Arbor, Michigan: Ann Arbor Science, 1979.

Congress, Library of. "H.R. 6 Clean Energy Act of 2007 (Introduced to House)." *Thomas.* 2007. http://thomas.loc.gov/cgi-bin/query/D?c110:1:./temp/~c110WFDyHR:: (accessed 2009).

—. "S.1630 Clean Air Amendments of 1990 (Public Print)." *Thomas.* 1990. http://thomas.loc.gov/cgi-bin/query/D?c101:4:./temp/~c1015BBiZ3:: (accessed 2010).

Conservation Reserve Program. *Summary of Enrollment Statistics.* USDA Farm Service Agency, 2007.

Ethanol Renewable Fuels Association. *Industry Statistics.* 2005-2010. http://www.ethanolrfa.org/industry/statistics/#C (accessed April 1, 2010).

ExxonMobil. *Algae Biofuels.* 2009. http://exxonmobil.com/algae (accessed January 25, 2010).

Farabee, M. J. *Celular Metabolism and Fermentation.* 2007. http://www.emc.maricopa.edu/faculty/farabee/BIOBK/BioBookGlyc.html (accessed September 20, 2009).

Felder, Richard M, and Ronald W Rousseau. *Elementary Principles of Chemical Processes.* 3rd Edition. Danvers, MA: Wiley, 2005.

Feng, Xianshe, and Robert Y.M. Huang. "Liquid Separation by Membrane Pervaporation: A Review." *Ind. Eng. Chem. Res.*, 1997: 1048-1066.

Gaskell, David R. *Introduction to thermodynamics of materials.* 4th Edition. New York: Taylor & Francis, 2008.

Giaya, Arjan, and Robert W. Thompson. "Water Confined in Cylindrical Micropores." *Journal of Chemical Physics*, 2002: 3464-3475.

Graboski, M.S. "Fossil Energy Use in the Manufacture of Corn Ethanol." *National Corn Growers Association*, 2002.

Greer, D. "Creating Cellulosic Ethanol: Spinning Straw into Fuel." *Harvesting Clean Energy.* April 2005. http://www.harvestcleanenergy.org/enews/enews_0505/enews_0505_Cellulosic_Ethanol.htm (accessed September 20, 2009).

Hamilton, T. "Dow to Test Algae Ethanol." *Technology Review Web site.* July 16, 2009. http://www.technologyreview.com/business/23009/ (accessed September 8, 2009).

Hammerschlag, Roal. "Ethanol's Energy Return on Investment: A Survey of the Literature 1990–Present." *Environmental Science & Technology* 40, no. 6 (2006): 744–1750.

Hardenberg, Horst O. *Samuel Morey and his atmospheric engine.* Warrendale, PA: Society of Automotive Engineers, 1992.

InflationData.com. *Historical Crude Oil Prices.* March 11, 2010. http://inflationdata.com/Inflation/Inflation_Rate/Historical_Oil_Prices_Table.asp (accessed 2010).

Kang, J. *Fermentation of Ethanol.* http:..www.andrew.cmu.edu/user/jitkang/Fermentation%20of%20Ethanol/Fermentation%20of%20Ethanol.htm (accessed September 20, 2009).

Kim, S, and B Dale. "Environmental aspects of ethanol derived from no-tilled corn grain:nonrenewable energy consumption and greenhouse gas emissions." *Biomass Bioenergy* 28 (2005): 475-489.

Kotdawala, Rasesh R. "Adsorption Studies of Hazardous Air Pollutants in Microporous Adsorbents using Statistical Mechanical and Molecular Simulation Techniques." PhD Dissertation, Chemical Engineering, Worcester Polytechnic Institute, Worcester, MA, 2007.

Kotdawala, Rasesh R., Kazantzis, Nikolaos, Thompson, Robert W. "Analysis of binary adsorption of polar and nonpolar molecules." *The Journal of Chemical Physics* 123 (December 2005).

Kotdawala, Rasesh R., Nikolaos Kazantzis, and Robert W. Thompson. "An application of mean-field perturbation theory for theadsorption of polar molecules in nanoslit-pores." *Journal of Mathematical Chemistry* 38, no. 3 (October 2005): 325-344.

Kranzberg, Melvin. *Technology and Culture: An Anthology.* New York: Schocken Books, 1972.

Krauss, Clifford, and Jad Mouawad. "Exxon Chief Cautions Against Rapid Action to Cut Carbon Emissions." *New York Times.* February 14, 2007. http://www.nytimes.com/2007/02/14/business/14exxon.html (accessed November 19, 2009).

Lawson, Keith W., and Douglas R. Lloyd. "Membrane Distillation." *Journal of Membrane Science* (Elsevier) 124 (1997): 1-25.

Lorenz, D, and D Morris. *How Much Energy Does It Take to Make a Gallon of Ethanol?* Washington, D.C., 1995.

Marland, G, and A.F. Turhollow. "CO2 emissions from the production and combustion of fuel ethanol from corn." *Energy* 16, no. 11-12 (1991): 1307-1316.

McKetta, John J., Cunningham, William A. *Encyclopedia of Chemical Processing and Design: Vol.19. Energy, costing thermal electric power plants to Ethanol.* New York: Marcel Dekker Inc., 1983.

McMahon, Tim. *What is the Inflation Adjusted Price of Corn?* July 16, 2008. http://inflationdata.com/inflation/inflation_Articles/Corn_Inflation.asp (accessed 2010).

Oikawa, Eizo, Michiko Shingai, Kiyashi Motomi, and Tashiki Aoki. "Pervaporation Separation of Water-Ethanol Mixture through the Membrane poly(thioether amide)s Prepared from Aromatic Amide and 1,40benzenedithiol." *Desalination*, 1995: 69-77.

Perry, Robert H., and Don White. *Perry's Chemical Engineering Handbook.* 6th Edition. New York: McGraw-Hill, 2003.

Pimentel, D, and T Patzek. "thanol production using corn, switchgrass, and wood; biodiesel production using soybean and sunflower." *Nat. Resour. Res.* 14, no. 1 (2005): 65-76.

Renewable Fuels Association. "Ethanol Industry Statistics." *Renewable Fuels Association Web site.* 2009. http://www.ethanolrfa.org/industry/statistics/ (accessed September 23, 2009).

Roberts, Joel. "Text of Bush's State of the Union Address." *CBS News.* January 23, 2007. http://www.cbsnews.com/stories/2007/01/23/politics/main2391957.shtml (accessed 2009).

Shappouri, H, J.A. Duffield, and M Wang. "The Energy Balance of Corn Ethanol: An Update." *Agricultural Economic Report* (United States Department of Agriculture), 2002.

Tomaszewska, M., M. Gryta, and M.W. Moraski. "Mass transfer of HCl and H2O across the hydrophobic membrane during membrane distillation." *Journal of Membrane Science* (Elsevier) 166 (2000): 149-157.

U.S. Department of Agriculture. *Corn Briefing Room.* March 27, 2009. http://www.ers.usda.gov/briefing/Corn/ (accessed September 28, 2009).

U.S. Department of Energy. *Bureau of Transportation Statistics.* 2007. http://www.bts.gov/publications/national_transportation_statistics/ (accessed 2010).

—. "U.S. Energy Data Book." 2008. http://cta.ornl.gov/data/chapter1.shtml (accessed 2010).

U.S. Department of Transportation. "Highway Statistics." *Motor Vehicle Fuel Consumption and Travel.* 1995-2007. http://www.bts.gov/publications/national_transportation_statistics/html/table_04_09.html (accessed March 23, 2009).

—. "Highway Statistics to 1995." *Motor Vehicle Fuel Consumption and Travel.* 1960-1994. http://www.bts.gov/publications/national_transportation_statistics/html/table_04_09.html (accessed March 23, 2009).

Vane, Leland M. "Separation Technologies for the Recovery and Dehydration of Alcohols from Fermentation Broths." *Biofuels, Bioproducts, Biorefining*, 2008: 553-588.

Wald, M. L. "Algae Farm Aims to Turn Carbon Dioxide Into Fuel." *The New York Times Web site.* June 29, 2009. http://www.nytimes.com/2009/06/29/business/energy-environment/29biofuel.html (accessed September 8, 2009).

Wee, Shin-Ling, Ching-Thian Tye, and Subhash Bhatia. "Membrane Separation Process-Pervaporation Through Zeolite Membrane." *Separation and Purification Technology*, 2008: 501-515.

Wheals, Alan E., Basso, Luiz C., Alves, Denise M. G., Amorim, Henrique V. "Fuel ethanol after 25 years." *TIBTECH*, 1999: 482-487.

8 Appendices

8.1 Raw Lab Data

Table 12: Water Contact Angles

	Water Contact Angles			
Sample				**Average**
Teflon				
100nm	144.84	146.34	145.32	146
220nm	145.54	145.87	144.38	145
450nm	145.72	142.59	148.45	146
Nylon				
220nm	142.37	146.76	145.85	145
450nm	145.77	143.62	142.11	144
Polypropylene				
100nm	142.45	145.67	143.78	144
220nm	143.2	145.47	143.73	144
450nm	149.34	142.89	145.3	146

Table 13: 100% EtOH Flux Data

	Run 1			Run 2			Run 3			Average
Sample	**Volume of Sample Collected (ml)**	**Collection Time (s)**	**Flux ($g/m^2/s$)**	**Volume of Sample Collected (ml)**	**Collection Time (s)**	**Flux ($g/m^2/s$)**	**Volume of Sample Collected (mL)**	**Collection Time (s)**	**Flux ($g/m^2/s$)**	**Flux ($g/m^2/s$)**
Teflon										
100nm	3	900	0.38	3.5	900	0.44	3.2	900	0.40	**0.41**
220nm	30	4560	0.75	8	900	1.01	7.3	900	0.92	**0.89**
450nm	20	2070	1.10	5	720	0.79	11	900	1.39	**1.09**
Nylon										
220nm	23	8880	0.29	3.8	900	0.48	2.8	900	0.35	**0.32**
450nm	20	1020	2.23	14	900	1.77	17	900	2.15	**2.05**
Polypropylene										
100nm	3	900	0.38	3.6	900	0.45	3.1	900	0.39	**0.41**
220nm	29	6480	0.51	4.3	900	0.54	4.7	900	0.59	**0.55**
450nm	14	2430	0.65	6.1	900	0.77	5.8	900	0.73	**0.72**

Table 14: 50/50 Mole% EtOH/Water Selectivity Data

	Feed			Run 1				Run 2				Average
Sample	**Density (g/mL)**	**Wt%**	**Mole%**	**Density (g/mL)**	**Wt%**	**Mole%**	**Selectivity**	**Density (g/mL)**	**Wt%**	**Mole%**	**Selectivity**	**Selectivity**
Teflon												
100nm	0.86	0.73	0.51	0.86	0.72	0.50	0.98	0.86	0.72	0.50	0.98	**0.98**
220nm	0.86	0.73	0.51	0.86	0.72	0.50	0.98	0.86	0.72	0.50	0.98	**0.98**
450nm	0.86	0.71	0.49	0.87	0.67	0.44	0.83	0.86	0.71	0.49	1.00	**0.92**
Nylon												
220nm	0.86	0.71	0.49	0.87	0.69	0.47	0.91	0.86	0.73	0.51	1.10	**1.01**
450nm	0.86	0.71	0.49	0.86	0.73	0.51	1.10	0.86	0.71	0.49	1.00	**1.05**
Polypropylene												
100nm	0.86	0.73	0.51	0.86	0.72	0.50	0.98	0.86	0.72	0.50	0.98	**0.98**
220nm	0.86	0.73	0.51	0.86	0.73	0.51	1.03	0.86	0.70	0.48	0.89	**0.96**
450nm	0.86	0.71	0.49	0.86	0.71	0.49	1.00	0.86	0.72	0.50	1.02	**1.01**

Table 15: 90/10 - EtOH/Water Selectivity Data

	Feed			Run 1				Run 2				Average
Sample	**Density (g/mL)**	**Wt%**	**Mole%**	**Density (g/mL)**	**Wt%**	**Mole%**	**Selectivity**	**Density (g/mL)**	**Wt%**	**Mole%**	**Selectivity**	**Selectivity**
Teflon												
100nm	0.80	0.96	0.90	0.80	0.96	0.91	1.03	0.80	0.96	0.91	1.08	**1.06**
220nm	0.80	0.96	0.90	0.80	0.96	0.91	1.03	0.80	0.96	0.90	0.93	**0.98**
450nm	0.80	0.96	0.90	0.80	0.96	0.91	1.05	0.80	0.96	0.91	1.05	**1.05**
Nylon												
220nm	0.80	0.96	0.90	0.80	0.96	0.90	1.00	0.80	0.96	0.91	1.05	**1.03**
450nm	0.80	0.96	0.90	0.80	0.96	0.90	0.93	0.80	0.96	0.90	0.97	**0.95**
Polypropylene												
100nm	0.80	0.96	0.90	0.80	0.96	0.91	1.03	0.80	0.96	0.90	0.97	**1.00**
220nm	0.80	0.96	0.90	0.80	0.96	0.90	1.00	0.80	0.96	0.91	1.08	**1.04**
450nm	0.80	0.96	0.90	0.80	0.96	0.91	1.08	0.80	0.96	0.89	0.88	**0.98**

8.2 Contact Angle Screenshots

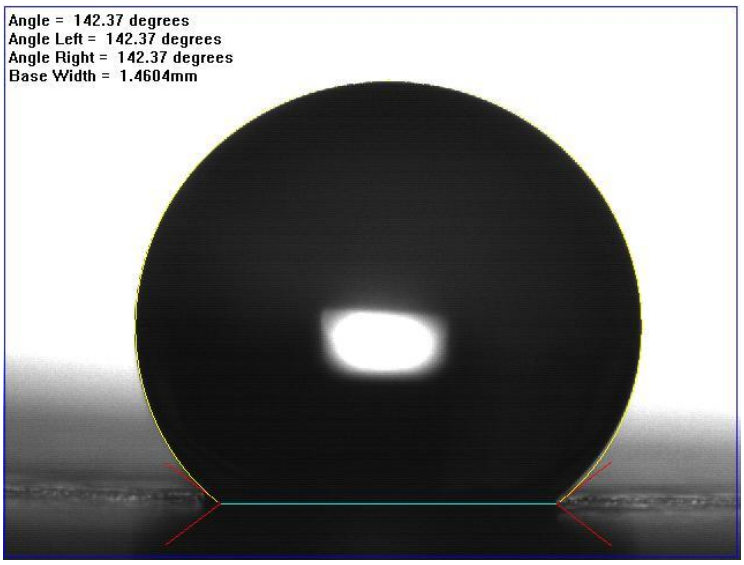

Figure 22: Nylon 220nm

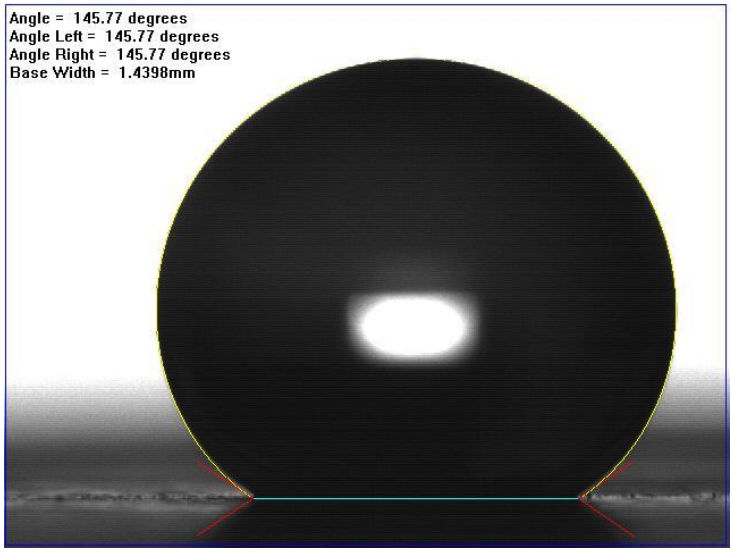

Figure 23: Nylon 450nm

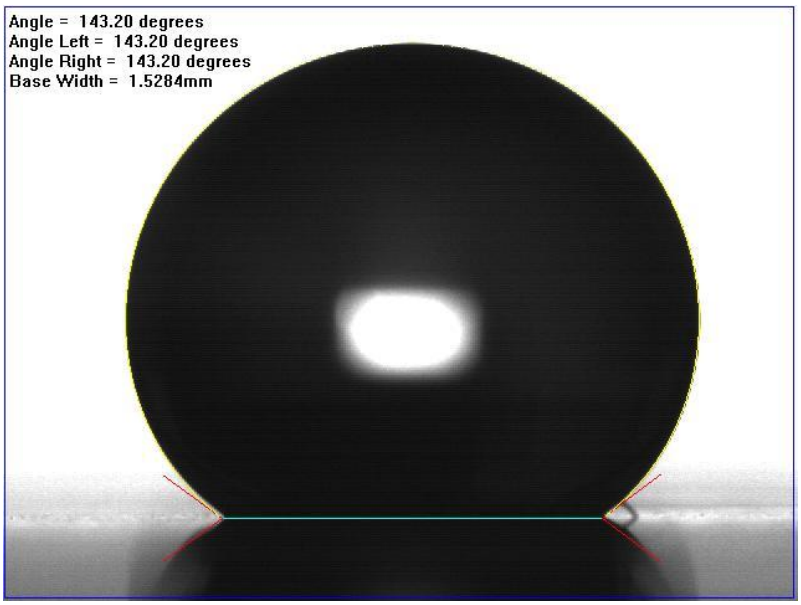

Figure 24: Polypropylene 220nm

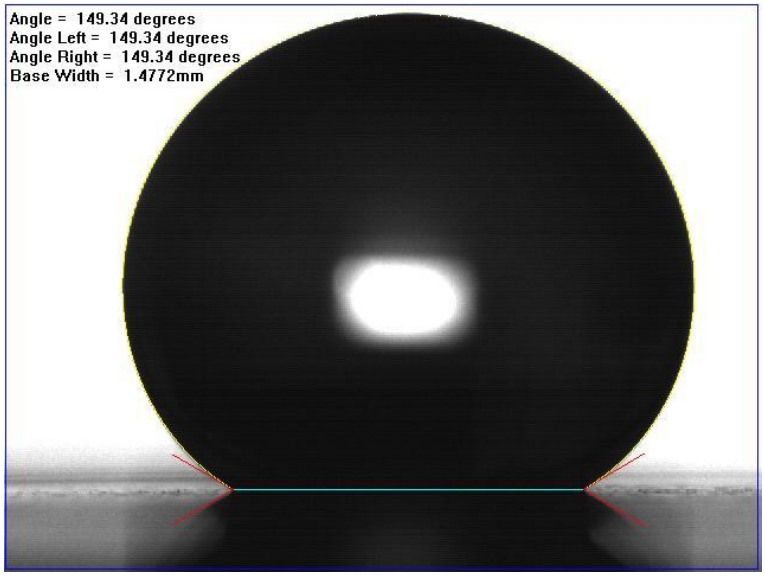

Figure 25: Polyproplyene 450nm

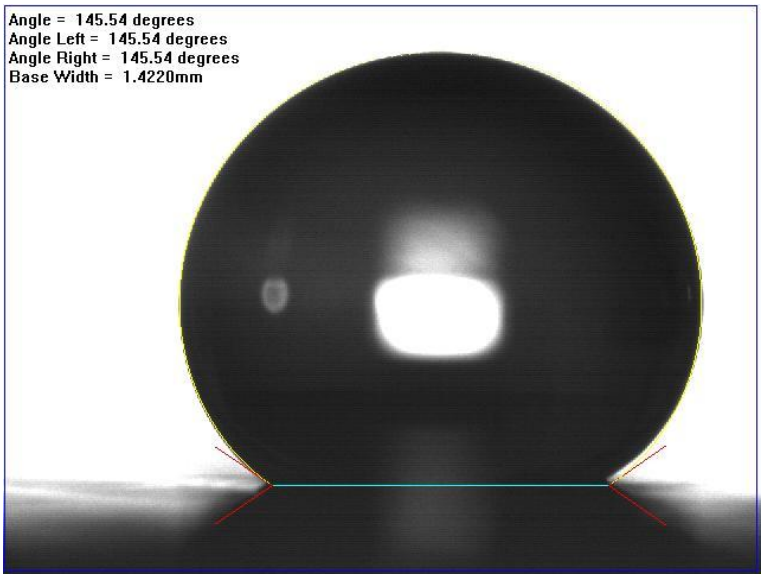

Figure 26: Teflon 220nm

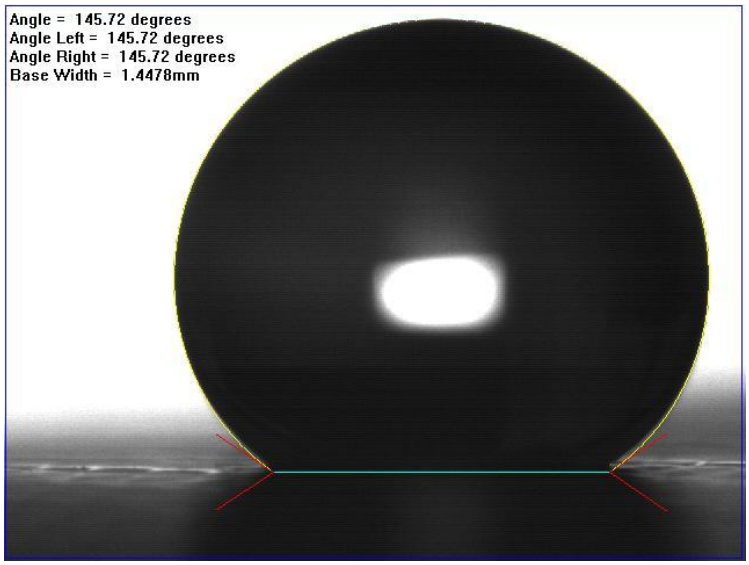

Figure 27: Teflon 450nm

8.3 Ethanol-Water Specific Gravity Table

wt % Ethanol	Temperature (degC)				wt % Ethanol	Temperature (degC)			
	20	25	30	35		20	25	30	35
0	0.99823	0.99708	0.99568	0.99406	50	0.91384	0.90985	0.90580	0.90168
1	0.99636	0.9952	0.99379	0.99217	51	0.91160	0.90760	0.90353	0.89940
2	0.99453	0.99336	0.99194	0.99031	52	0.90936	0.90534	0.90125	0.89710
3	0.99275	0.99157	0.99014	0.98849	53	0.90711	0.90307	0.89896	0.89479
4	0.99103	0.98984	0.98839	0.98672	54	0.90485	0.90079	0.89667	0.89248
5	0.98938	0.98817	0.98679	0.98501	55	0.90258	0.89850	0.89437	0.89016
6	0.9878	0.98656	0.98507	0.98335	56	0.90031	0.89621	0.89206	0.88784
7	0.98627	0.98500	0.98347	0.98172	57	0.89803	0.89392	0.88975	0.88552
8	0.98478	0.98346	0.98189	0.98009	58	0.89574	0.89162	0.88744	0.88319
9	0.98331	0.98193	0.98031	0.97846	59	0.89344	0.88931	0.88512	0.88085
10	0.98187	0.98043	0.97875	0.97685	60	0.89113	0.88699	0.88278	0.87851
11	0.98047	0.97897	0.97723	0.97527	61	0.88882	0.88446	0.88044	0.87615
12	0.97910	0.97753	0.97573	0.97371	62	0.88650	0.88233	0.87809	0.87379
13	0.97775	0.97661	0.97424	0.97216	63	0.88417	0.87998	0.87574	0.87142
14	0.97643	0.97472	0.97278	0.97063	64	0.88183	0.87763	0.87337	0.86905
15	0.97514	0.97334	0.97133	0.96911	65	0.87948	0.87527	0.87100	0.86667
16	0.97387	0.97199	0.96990	0.9676	66	0.87713	0.87291	0.86863	0.86429
17	0.97259	0.97062	0.96844	0.96607	67	0.87477	0.87054	0.86625	0.86190
18	0.97129	0.96923	0.96697	0.96452	68	0.87241	0.86817	0.86387	0.85950
19	0.96997	0.96782	0.96547	0.96294	69	0.87004	0.86579	0.86148	0.85710
20	0.96864	0.96639	0.96395	0.96134	70	0.86766	0.86340	0.85908	0.85470
21	0.96729	0.96495	0.96242	0.96973	71	0.86527	0.86100	0.85667	0.85228
22	0.96592	0.96348	0.96087	0.95809	72	0.86287	0.85859	0.85426	0.84986
23	0.96453	0.96199	0.95929	0.95643	73	0.86047	0.85618	0.85184	0.84743
24	0.96312	0.96048	0.95769	0.95476	74	0.85806	0.85376	0.84941	0.84500
25	0.96168	0.95895	0.95607	0.95306	75	0.85564	0.85134	0.84698	0.84257
26	0.96020	0.95738	0.95442	0.95133	76	0.85322	0.84891	0.84455	0.84013
27	0.95867	0.95576	0.95272	0.94995	77	0.85079	0.84647	0.84211	0.83768
28	0.95710	0.95410	0.95098	0.95774	78	0.84835	0.84403	0.83966	0.83523
29	0.95548	0.95241	0.94922	0.94590	79	0.84590	0.84158	0.83720	0.83277
30	0.95382	0.95067	0.94741	0.94403	80	0.84344	0.83911	0.83473	0.83029
31	0.95212	0.94890	0.94557	0.94214	81	0.84096	0.83664	0.83224	0.82780
32	0.95038	0.94709	0.94370	0.94021	82	0.83848	0.83415	0.82974	0.82530
33	0.94860	0.94525	0.94180	0.93825	83	0.83599	0.83164	0.82724	0.82279
34	0.94679	0.94337	0.93986	0.93626	84	0.83348	0.82913	0.82473	0.82027
35	0.94494	0.94146	0.93790	0.93425	85	0.83095	0.82660	0.82220	0.81774
36	0.94306	0.93952	0.93591	0.93221	86	0.82840	0.82405	0.81965	0.81519
37	0.94114	0.93756	0.93390	0.93016	87	0.82583	0.82148	0.81708	0.81262
38	0.93919	0.93556	0.93186	0.92808	88	0.82323	0.81888	0.81448	0.81003
39	0.93720	0.93353	0.92979	0.92597	89	0.82062	0.81626	0.81186	0.80742
40	0.93518	0.93148	0.92770	0.92385	90	0.81797	0.81362	0.80922	0.80478
41	0.93314	0.92940	0.92558	0.92170	91	0.81529	0.81094	0.80655	0.80211
42	0.93107	0.92729	0.92344	0.91952	92	0.81257	0.80823	0.80384	0.79941
43	0.92897	0.92516	0.92128	0.91733	93	0.80983	0.80549	0.80111	0.79669
44	0.92685	0.92301	0.91910	0.91513	94	0.80705	0.80272	0.79835	0.79393
45	0.92472	0.92085	0.91692	0.91291	95	0.80424	0.79991	0.79555	0.79114
46	0.92257	0.91868	0.91472	0.91069	96	0.80138	0.79706	0.79271	0.78831
47	0.92041	0.91649	0.91250	0.90845	97	0.79846	0.79415	0.78991	0.78542
48	0.91823	0.91426	0.91028	0.90621	98	0.79547	0.79117	0.78684	0.78247
49	0.91604	0.91208	0.90805	0.90396	99	0.79543	0.78814	0.78382	0.77946
					100	0.78934	0.78506	0.78075	0.77641

Figure 28: Concentration of EtOH in weight percent of EtOH-Water Mixture versus Specific Gravity at Various Temperatures (Perry and White 2003)

8.4 SEM Images

Provided in this section are the SEM pictures of the 3 different types of membranes and the 2 different pore sizes. The left hand pictures show fresh membranes out of packaging while the pictures on the right were samples that were used with 50-50 mixtures of ethanol and water. After being exposed to the 50-50 mixtures the membranes were allowed to air dry before going through the SEM imaging process.

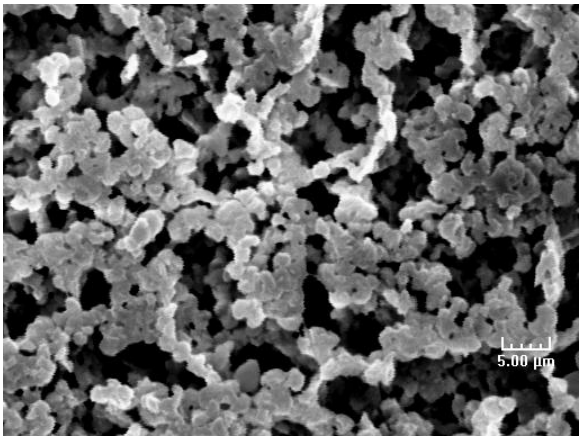

Figure 29: Dry Nylon 450nm - 2000X

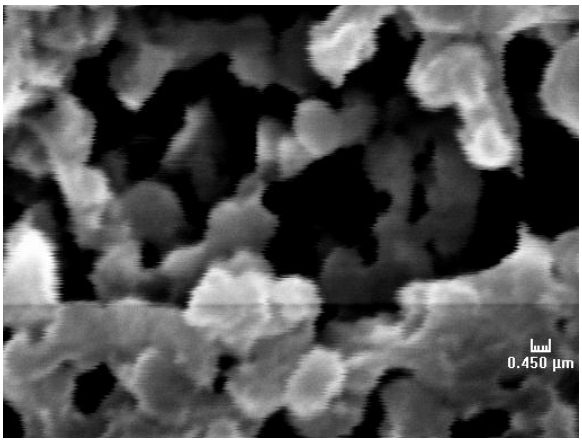

Figure 30: Nylon 450nm - 7000X

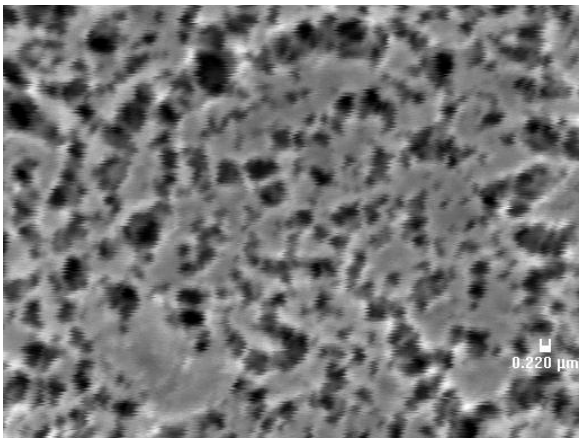

Figure 31: Dry Polypropylene 220nm - 7000X

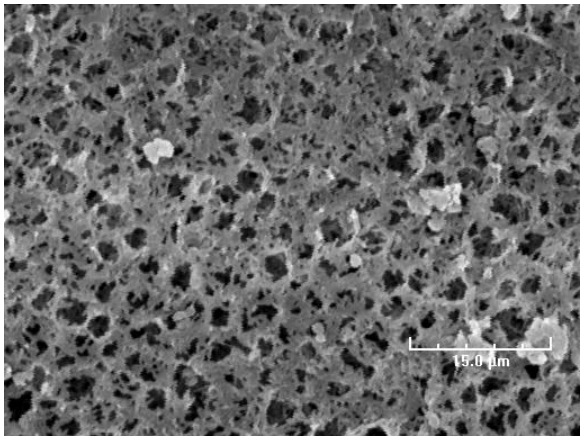

Figure 32: Soaked Nylon 450nm - 2000X

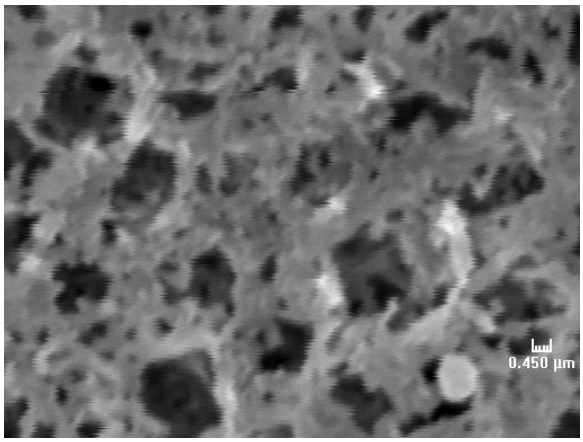

Figure 33: Soaked Nylon 450nm - 7000X

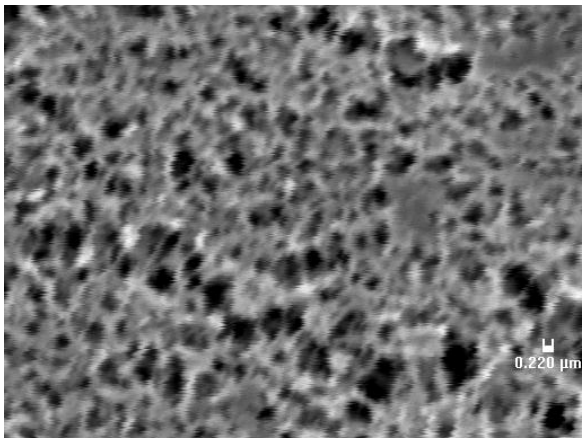

Figure 34: Soaked Polypropylene 220nm - 7000X

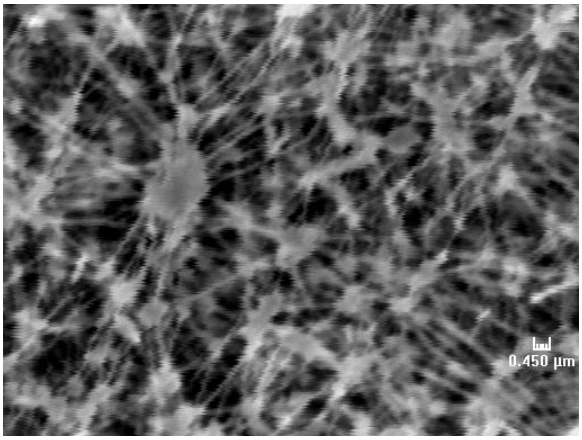

Figure 35: Dry Teflon 450nm - 6000X

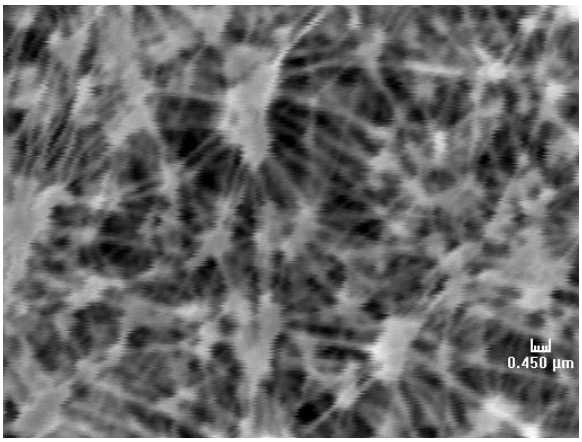

Figure 36: Dry Teflon 450nm - 7000X

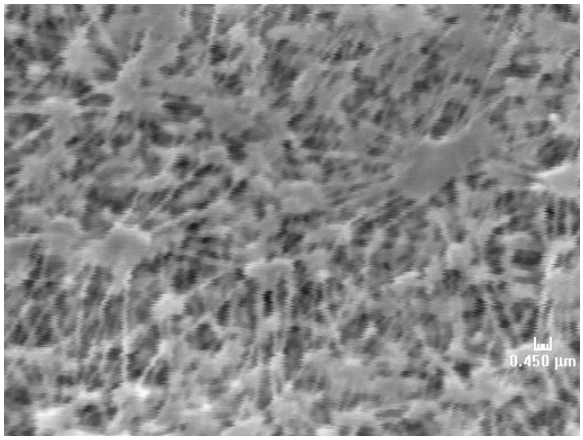

Figure 37: Soaked Teflon 450nm - 6000X

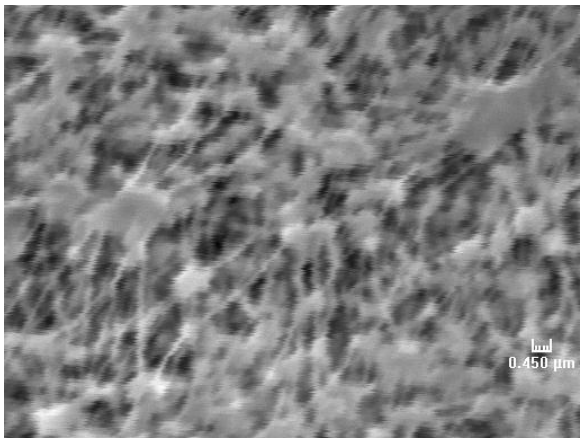

Figure 38: Soaked Teflon 450nm - 7000X

8.5 MATLAB Code

8.5.1 Raw MATLAB Code

```
% sz=15A onwards
%function F = myfun(x)
%syms z sif1 sif2 sz  ros esf1 esf2;
k=1.38*10^-23;
h=6.64*10^-34;
N=6.02*10^23;
m1=18.02*10^-3/N;
m2=32.04*10^-3/N;
d=3.35e-10;
T=298;
ef1=80*k;
ef2=97.4*k;
sf=3.4*10^-10;
esf1=47.32*k;
esf2=52.22*k;
ros=1.14*10^29;
sz=18*10^-10;
m=input('m');
rob1=m*.5*1e+25;
rob2=m*.5*1e+25;
si1=3.1*(10^-10);
si2=3.42*10^-10;
sif1=0.5*(sf+si1);
sif2=0.5*(sf+si2);
laba1=(h^2/(2*3.14*m1*k*T))^0.5;
laba2=(h^2/(2*3.14*m2*k*T))^0.5;
zeta1=sz/si1;
zeta2=sz/si2;
I1=2*10^-18;
I2=1.7*10^-18;
mu1=1.9*3.3*10^-30;
```

```
mu2=1.7*3.3*10^-30;
ee=8.85*10^-12;
al1=1.5*10^-30*4*3.18*ee;
al2=3.4*10^-30*4*3.18*ee;
bb1=(1/(1.5))*si1^3*3.14;
bb2=(1/(1.5))*si2^3*3.14;
bp1=bb1*(1-(3/(16*zeta1)));
bp2=bb2*(1-(3/(16*zeta2)));
beta=1/(1.38*10^-23*T);
%m1= ((-2*sif1^10)/(9*(sz-sif1)^9))-((4/9)*sif1)+((0.666*sif1^4)/(sz-sif1)^3)+((2*1666.6*sif1^4)/(d*((61*d)+(100*sz)-
(100*sif1))^2))-((2*1666.7*sif1^4)/(d*((61*d)+(100*sif1))^2));
%n1=6.28*d*esf1*ros*sif1^2;
%s1=(2*n1*m1/(sz-sif1));
%m2= ((-2*sif2^10)/(9*(sz-sif2)^9))-((4/9)*sif2)+((0.666*sif2^4)/(sz-sif2)^3)+((2*1666.6*sif2^4)/(d*((61*d)+(100*sz)-
(100*sif2))^2))-((2*1666.7*sif2^4)/(d*((61*d)+(100*sif2))^2));
%n2=6.28*d*esf2*ros*sif2^2;
%s2=(2*n2*m2/(sz-sif2));
s1=((6.28*1.63*ros*esf1*sif1^3)/(3*1*(zeta1-2)))*((1/(zeta1-1)^2)-1);%(zeta>2)
s2=((6.28*1.63*ros*esf2*sif2^3)/(3*1*(zeta2-2)))*((1/(zeta2-1)^2)-1);%(zeta>2)
rop1=1.1e29;
rop2=1.10e2;
for i=1:1000,
ap11=(((0.66*mu1^4)/(k*T))+(2*mu1^2*al1)+(0.75*al1^2*I1))/(4*3.14*ee)^2;
ap22=(((0.66*mu2^4)/(k*T))+(2*mu2^2*al2)+(0.75*al2^2*I2))/(4*3.14*ee)^2;
ap12=(((0.66*mu1^2*mu2^2)/(k*T))+(2*(mu1^2*al1+mu2^2*al2))+((0.75*al1*al2*I1*I2)/(I1+I2)))/(4*3.14*ee)^2;
ap1=1*((2*3.14*ap11)/(3*si1^3))*(((-1.5*si1)+(2*(sz-(2*sif1)))+(si1^3/(4*(sz-(2*sif1))^2)))/(sz-(2*sif1)));
ap2=1*((2*3.14*ap22)/(3*si2^3))*(((-1.5*si2)+(2*(sz-(2*sif2)))+(si2^3/(4*(sz-(2*sif2))^2)))/(sz-(2*sif2)));
ap121=1.2*((2*3.14*ap12)/(3*si2^3))*(((-1.5*si2)+(2*(sz-(2*sif2)))+(si2^3/(4*(sz-(2*sif2))^2)))/(sz-(2*sif2)));
ab1=1*((4*3.18)/((si1^3)*3))*ap11;
ab2=1*((4*3.18)/((si2^3)*3))*ap22;
ab121=1*((4*3.18)/((si2^3)*3))*ap12;
mu1=((6e-29*rop1)+1.9)*3.3e-30;
mu2=((6e-29*rop2)+1.71)*3.3e-30;
F1=((-1)*(((-bp1*(rop1+rop2))/(1-rop1*bp1-rop2*bp2))+(log(1-rop1*bp1-rop2*bp2))-(log(rop1*laba1^3))))+(beta*s1)-
(beta*2*ap1*rop1)+(((-bb1*(rob1+rob2))/(1-rob1*bb1-rob2*bb2))+(log(1-rob1*bb1-rob2*bb2))-
(log(rob1*laba1^3)))+(2*beta*ab1*rob1);
F2=((-1)*(((-bp2*(rop1+rop2))/(1-rop1*bp1-rop2*bp2))+(log(1-rop1*bp1-rop2*bp2))-(log(rop2*laba2^3))))+(s2*beta)-
(beta*2*ap2*rop2)-(beta*2*ap121*rop2)+(((-bb2*(rob1+rob2))/(1-rob1*bb1-rob2*bb2))+(log(1-rob1*bb1-rob2*bb2))-
```

```
(log(rob2*laba2^3)))+(2*beta*ab2*rob2)+(2*beta*ab121*rob2);

%F1=-(1/beta)*(((-bp1*(rop1+rop2))/(1-rop1*bp1-rop2*bp2))+(log(1-rop1*bp1-rop2*bp2))-(log(rop1*laba1)))+s1+(2*ap1*rop1);

%F2=-(1/beta)*(((-bp2*(rop1+rop2))/(1-rop1*bp1-rop2*bp2))+(log(1-rop1*bp1-rop2*bp2))-(log(rop2*laba2)))+s2+(2*ap2*rop2);
df1rop1=((-1)*(((((1-rop1*bp1-rop2*bp2)*(-bp2))-((-bp1)^2*(rop1+rop2)))/(1-rop1*bp1-rop2*bp2)^2)-(bp1/(1-rop1*bp1-
rop2*bp2)^2)-(1/rop1)))-(beta*2*ap1);
df1rop2=((-1)*(((((1-rop1*bp1-rop2*bp2)*(-bp2))-((-bp2)^2*(rop1+rop2)))/(1-rop1*bp1-rop2*bp2)^2)-(bp2/(1-rop1*bp1-
rop2*bp2)^2)));
df2rop1=((-1)*(((((1-rop1*bp1-rop2*bp2)*(-bp2))-((bp2)*(-bp1)*(rop1+rop2)))/(1-rop1*bp1-rop2*bp2)^2)-(bp1/(1-rop1*bp1-
rop2*bp2)^2)));
df2rop2=((-1)*(((((1-rop1*bp1-rop2*bp2)*(-bp2))-((-bp2)^2*(rop1+rop2)))/(1-rop1*bp1-rop2*bp2)^2)-(bp2/(1-rop1*bp1-
rop2*bp2)^2)-(1/rop2)))-(beta*2*ap2)-(beta*2*ap121);

h=-(real(-(F2)*df1rop2)+(df2rop2*real(F1)))/(((df1rop1*df2rop2)-(df1rop2*df2rop1)));

k1=((real(F1)*df2rop1)-(df1rop1*real(F2)))/(((df1rop1*df2rop2)-(df1rop2*df2rop1)));

real(F1);

real(F2);

rop1=(h)+rop1;

rop2=(k1)+rop2;

(h*df1rop1)+(k1*df1rop2);

(h*df2rop1)+(k1*df2rop2);

end

s=(rop2/rob2)/(rop1/rob1)

rop1

rop2

xp1=rop1/(rop1+rop2)

xp2=rop2/(rop1+rop2)

efm=s1*N

efem=s2*N

water=ap1*rop1*N

methane=ap2*rop2*N

methanewater=ap121*rop2*N

F1

F2

xb1=rob1/(rob1+rob2);

xb2=rob2/(rob1+rob2);

rob1;

rob2;

s=exp(-s2/(k*T))/exp(-s1/(k*T));

potent=((-N*k*T*(1+bp1*rop1+bp2*rop2))/(1-(bp1*rop1-bp2*rop2)))+(N*ap1*xp1*rop1)+(N*rop2*xp2*ap2)+(N*rop2*xp2*ap121)
```

```
98  (N*ap1*xp1*rop1);
99  (N*rop2*xp2*ap2);
100 (N*rop2*xp2*ap121);
101 1/bp2;
102 mu1/3.3e-30
103 mu2/3.3e-30
```

8.5.2 MATLAB Simulation Equations

For the readers convenience the complex equations found within the raw matlab code are reproduced in an easier to read format.

MATLAB Line 25:

$$laba1 = \sqrt{\frac{\mathrm{h}^2}{2\pi * \text{mass comp } 2 * \mathrm{k} * \mathrm{T}}}$$

MATLAB Line 26

$$\text{laba2} = \left(\frac{\mathrm{h}^2}{2 * 3.14 * \mathrm{m2} * \mathrm{k} * \mathrm{T}}\right)^{0.5}$$

MATLAB Line 47

$$\mathrm{s1} = \frac{6.28 * 1.63 * \rho_s * \mathrm{esf1} * \mathrm{sif1}^3}{3 * 1 * \mathrm{zeta1} - 2} * \left(\frac{1}{(\mathrm{zeta1} - 1)^2}\right) - 1$$

MATLAB Line 48

$$\mathrm{s2} = \left(\frac{6.28 * 1.63 * \mathrm{ros} * \mathrm{esf2} * \mathrm{sif2}^3}{3 * 1 * (\mathrm{zeta2} - 2)}\right) * \left(\left(\frac{1}{(\mathrm{zeta2} - 1)^2}\right) - 1\right)$$

MATLAB Lines 52

$$\mathrm{ap11} = \frac{\left(\frac{0.66 * \mathrm{mu1}^4}{\mathrm{k} * \mathrm{T}}\right) + (2 * \mathrm{mu1}^2 * \mathrm{al1}) + (0.75 * \mathrm{al1}^2 * \mathrm{I1})}{(4 * 3.14 * \mathrm{ee})^2}$$

MATLAB Line 53

$$\mathrm{ap22} = \frac{\left(\frac{0.66 * \mathrm{mu2}^4}{\mathrm{k} * \mathrm{T}}\right) + (2 * \mathrm{mu2}^2 * \mathrm{al2}) + (0.75 * \mathrm{al2}^2 * \mathrm{I2})}{(4 * 3.14 * \mathrm{ee})^2}$$

MATLAB Lines 54

$$ap11 = \left(\frac{0.66 * mu1^4}{kT}\right) + (2 * mu1^2 * al1) + \frac{0.75 * al1^2 * I1 * I2}{\frac{I1 + I2}{(4 * 3.14 * ee)^2}}$$

MATLAB Lines 55

$$ap1 = 1 * \left(\frac{2 * \pi * ap11}{3 * si1^3}\right) * \left(\frac{(-1.5 * si1) + \left(2 * \left(sz - (2 * sif1)\right)\right) + \left(\frac{si1^3}{4 * \left(sz - (2 * sif1)\right)^2}\right)}{sz - (2 * sif1)}\right)$$

MATLABE Line 56

$$\mathrm{ap2} = 1 * \left(\frac{2 * 3.14 * \mathrm{ap22}}{3 * \mathrm{si2}^3}\right) * \left(\frac{(-1.5 * \mathrm{si2}) + \left(2 * \left(\mathrm{sz} - (2 * \mathrm{sif2})\right)\right) + \left(\frac{\mathrm{si2}^3}{4 * \left(\mathrm{sz} - (2 * \mathrm{sif2})\right)^2}\right)}{\mathrm{sz} - (2 * \mathrm{sif2})}\right)$$

MATLAB Line 57

$$\mathrm{ap121} = 1.2 * \left(\frac{2 * 3.14 * \mathrm{ap12}}{3 * \mathrm{si2}^3}\right) * \left(\frac{(-1.5 * \mathrm{si2}) + \left(2 * \left(\mathrm{sz} - (2 * \mathrm{sif2})\right)\right) + \left(\frac{\mathrm{si2}^3}{4 * \left(\mathrm{sz} - (2 * \mathrm{sif2})\right)^2}\right)}{\mathrm{sz} - (2 * \mathrm{sif2})}\right)$$

MATLAB Line 58

$$ab1 = 1 * \left(\frac{4 * 3.18}{(si1^3) * 3}\right) * ap11$$

MATLAB Line 59

$$\mathrm{ab2} = 1 * \left(\frac{4 * 3.18}{(\mathrm{si2}^3) * 3}\right) * \mathrm{ap22}$$

MATLAB Line 60

$$ab121 = 1 * \left(\frac{4 * 3.18}{(si2^3) * 3}\right) * ap12$$

MATLAB Line 61

$$mu1 = \left((6 * 10^{29} * rop1) + 1.9\right) * 3.3 * 10^{-30}$$

MATLAB Line 62

$$mu2 = \left((6 * 10^{29} * rop2) + 1.71\right) * 3.3 * 10^{-30}$$

MATLAB Line 63

$$F1 = \left((-1) * \left(\left(\frac{-bp1 * (rop1 + rop2)}{1 - rop1 * bp1 - rop2 * bp2}\right) + (\ln(1 - rop1 * bp1 - rop2 * bp2)) - (\ln(rop1 * laba1^3))\right)\right) + (beta * s1) - (beta * 2 * ap1 * rop1)$$
$$+ \left(\left(\frac{-bb1 * (rob1 + rob2)}{1 - rob1 * bb1 - rob2 * bb2}\right) + (\ln(1 - rob1 * bb1 - rob2 * bb2)) - (\ln(rob1 * laba1^3))\right) + (2 * beta * ab1 * rob1)$$

MATLAB Line 64

$$\mathrm{F2} = \left((-1) * \left(\left(\frac{-\mathrm{bp2} * (\mathrm{rop1} + \mathrm{rop2})}{1 - \mathrm{rop1} * \mathrm{bp1} - \mathrm{rop2} * \mathrm{bp2}}\right) + \left(\ln(1 - \mathrm{rop1} * \mathrm{bp1} - \mathrm{rop2} * \mathrm{bp2})\right) - \left(\ln(\mathrm{rop2} * \mathrm{laba2}^3)\right)\right)\right) + (\mathrm{s2} * \mathrm{beta}) - (\mathrm{beta} * 2 * \mathrm{ap2} * \mathrm{rop2}) - (\mathrm{beta} * 2 * \mathrm{ap121} * \mathrm{rop2})$$
$$+ \left(\left(\frac{-\mathrm{bb2} * (\mathrm{rob1} + \mathrm{rob2})}{1 - \mathrm{rob1} * \mathrm{bb1} - \mathrm{rob2} * \mathrm{bb2}}\right) + \left(\ln(1 - \mathrm{rob1} * \mathrm{bb1} - \mathrm{rob2} * \mathrm{bb2})\right) - \left(\ln(\mathrm{rob2} * \mathrm{laba2}^3)\right)\right) + (2 * \mathrm{beta} * \mathrm{ab2} * \mathrm{rob2}) + (2 * \mathrm{beta} * \mathrm{ab121} * \mathrm{rob2})$$

MATLAB Line 67

$$\mathrm{df1rop1} = \left((-1) * \left(\left(\frac{\left((1 - \mathrm{rop1} * \mathrm{bp1} - \mathrm{rop2} * \mathrm{bp2}) * (-\mathrm{bp2})\right) - \left((-\mathrm{bp1})^2 * (\mathrm{rop1} + \mathrm{rop2})\right)}{(1 - \mathrm{rop1} * \mathrm{bp1} - \mathrm{rop2} * \mathrm{bp2})^2}\right) - \left(\frac{\mathrm{bp1}}{(1 - \mathrm{rop1} * \mathrm{bp1} - \mathrm{rop2} * \mathrm{bp2})^2}\right) - \left(\frac{1}{\mathrm{rop1}}\right)\right)\right) - (\mathrm{beta} * 2 * \mathrm{ap1})$$

MATLAB Line 68

$$\mathrm{df1rop2} = \left((-1) * \left(\left(\frac{\left((1 - \mathrm{rop1} * \mathrm{bp1} - \mathrm{rop2} * \mathrm{bp2}) * (-\mathrm{bp2})\right) - \left((-\mathrm{bp2})^2 * (\mathrm{rop1} + \mathrm{rop2})\right)}{(1 - \mathrm{rop1} * \mathrm{bp1} - \mathrm{rop2} * \mathrm{bp2})^2}\right) - \left(\frac{\mathrm{bp2}}{(1 - \mathrm{rop1} * \mathrm{bp1} - \mathrm{rop2} * \mathrm{bp2})^2}\right)\right)\right)$$

MATLAB Line 69

$$\mathrm{df2rop1} = \left((-1) * \left(\left(\frac{\left((1 - \mathrm{rop1} * \mathrm{bp1} - \mathrm{rop2} * \mathrm{bp2}) * (-\mathrm{bp2})\right) - \left((\mathrm{bp2}) * (-\mathrm{bp1}) * (\mathrm{rop1} + \mathrm{rop2})\right)}{(1 - \mathrm{rop1} * \mathrm{bp1} - \mathrm{rop2} * \mathrm{bp2})^2}\right) - \left(\frac{\mathrm{bp1}}{(1 - \mathrm{rop1} * \mathrm{bp1} - \mathrm{rop2} * \mathrm{bp2})^2}\right)\right)\right)$$

MATLAB Line 70

$$\mathrm{df2rop2} = \left((-1) * \left(\left(\frac{\left((1 - \mathrm{rop1} * \mathrm{bp1} - \mathrm{rop2} * \mathrm{bp2}) * (-\mathrm{bp2})\right) - \left((-\mathrm{bp2})^2 * (\mathrm{rop1} + \mathrm{rop2})\right)}{(1 - \mathrm{rop1} * \mathrm{bp1} - \mathrm{rop2} * \mathrm{bp2})^2}\right) - \left(\frac{\mathrm{bp2}}{(1 - \mathrm{rop1} * \mathrm{bp1} - \mathrm{rop2} * \mathrm{bp2})^2}\right) - \left(\frac{1}{\mathrm{rop2}}\right)\right)\right) - (\mathrm{beta} * 2 * \mathrm{ap2}) - (\mathrm{beta} * 2 * \mathrm{ap121})$$

MATLAB Line 71

$$\mathrm{h} = -\frac{\mathrm{real}(-(\mathrm{F2}) * \mathrm{df1rop2}) + \left(\mathrm{df2rop2} * \mathrm{real}(\mathrm{F1})\right)}{\left((\mathrm{df1rop1} * \mathrm{df2rop2}) - (\mathrm{df1rop2} * \mathrm{df2rop1})\right)}$$

MATLAB Line 72

$$\mathrm{k1} = \frac{(\mathrm{real}(\mathrm{F1}) * \mathrm{df2rop1}) - \left(\mathrm{df1rop1} * \mathrm{real}(\mathrm{F2})\right)}{\left((\mathrm{df1rop1} * \mathrm{df2rop2}) - (\mathrm{df1rop2} * \mathrm{df2rop1})\right)}$$

MATLAB Line 75

$$rop1 = h + rop1$$

MATLAB Line 76

$$rop2 = h + rop2$$

MATLAB Line 77

$$(h * df1rop1) + (k1 * df1rop2)$$

MATLAB Line 78

(h*df2rop1)+(k1*df2rop2)

8.5.3 Tabulated Constants and Modified MATLAB Code Parameters

Table 16: MATLAB Parameters

MATLAB Variable	Definition	MATLAB Value	Units	Range Tested
k	Boltzmann Constant	1.38*10^-23	J/K	-
h	Planck's constant	6.64*10^-34	J*s	-
N	Avogadro's number	6.02*10^23	N/A	-
m1	molecule mass (comp.1)	18.02*10^-3/N	Kg/molecule	-
m2	molecule mass (comp. 2)	32.04*10^-3/N	Kg/molecule	-
d	distance between 2 wall atoms	3.35*10^-10	meters	-
T	Temperature	298	K	-
ef1	Fluid-Wall Interactions	80*k	-	-
ef2	Fluid-Wall Interactions	97.4*k	-	-
sf	Fluid-Wall Interactions	3.4*10^-10	meters	-
esf1	Fluid-Wall Interactions	47.32*k	-	0 - 100
esf2	Fluid-Wall Interactions	52.22*k	-	0 - 100
ros	aerial density of the solid substrate	1.14*10^29	-	-
sz	slit pore width	20*10^-10	meters	18 - 4500
m	bulk pressure	**INPUT**	Pa	0.006-4000
rob1	bulk density (comp. 1)	m*.5*1e+25	Molecules/m^3	-
rob2	bulk density (comp. 2)	m*.5*1e+25	Molecules/m^3	-
si1	Fluid-Wall Interactions	3.11*10^-10	meters	-
si2	Fluid-Wall Interactions	3.4225*10^-10	meters	-
I1	Fluid-Fluid Interactions (comp. 1)	2*10^-18	N/A	-
I2	Fluid-Fluid Interactions (comp. 2)	1.7*10^-18	N/A	-
mu1	Fluid-Fluid Interactions (comp. 1)	1.9*3.3*10^-30	Coulomb*meters	-
mu2	Fluid-Fluid Interactions (comp. 2)	1.7*3.3*10^-30	Coulomb*meters	-
al1	Fluid-Fluid Interactions (comp. 1)	1.5*10^-30*4*3.18*ee	N/A	-
al2	Fluid-Fluid Interactions (comp. 2)	3.4*10^-30*4*3.18*ee	N/A	-
rop1	Pore density (comp 1)	**USER GUESS**	Molecules/m^3	-
rop2	Pore density (comp 2)	**USER GUESS**	Molecules/m^3	-
s	Selectivity	**OUTPUT**	N/A	-
xp1	Pore phase mole fract. (comp. 1)	**OUTPUT**	N/A	-
xp2	Pore phase mole fract. (comp. 2)	**OUTPUT**	N/A	-
xb1	Bulk phase mole fract. (comp. 1)	**OUTPUT**	N/A	-
xb2	Bulk phase mole fract. (comp. 2)	**OUTPUT**	N/A	-

8.5.4 MATLAB Result Tables

Table 17: 1.8nm, esf1=0*k, esf2=74.22*k

sz	18																	
esf1	65.32																	
esf2	74.22																	
rop1 guess	1.00E+20	1.00E+20	1.00E+20	1.00E+20	1.00E+20	1.00E+20	1.00E+20	1.00E+20	1.00E+20	1.00E+20	1.00E+20	1.00E+20	1.00E+20	1.00E+20	1.00E+20	1.00E+20	1.00E+20	
rop2 guess	1.00E+20	1.00E+20	1.00E+20	1.00E+20	1.00E+20	1.00E+20	1.00E+20	1.00E+20	1.00E+20	1.00E+20	1.00E+20	1.00E+20	1.00E+20	1.00E+20	1.00E+20	1.00E+20	1.00E+20	
m	0.006	0.007	0.008	0.009	0.01	1	10	15	350	400	450	500	600	700	800	900	925	
rob	3.00E+22	3.50E+22	4.00E+22	4.50E+22	5.00E+22	5.00E+24	5.00E+25	7.50E+25	1.75E+27	2.00E+27	2.25E+27	2.50E+27	3.00E+27	3.50E+27	4.00E+27	4.50E+27	4.63E+27	
rop1	6.26E+22	7.30E+22	8.35E+22	9.39E+22	1.04E+23	1.05E+25	1.08E+26	1.63E+26	5.87E+26	3.96E+26	2.94E+26	2.27E+26	1.45E+26	9.98E+25	7.62E+25	6.80E+25	6.86E+25	
rop2	9.13E+22	1.06E+23	1.22E+23	1.37E+23	1.52E+23	1.54E+25	1.87E+26	3.63E+26	8.66E+25	5.64E+25	3.65E+25	2.37E+25	1.03E+25	4.79E+24	2.48E+24	1.55E+24	1.44E+24	
potent	-2476	-2476	-2476	-2476	-2476	-2450	-2149	-1809	-1723	-1978	-2106	-2189	-2290	-2346	-2375	-2385	-2384	
s	1.46	1.46	1.46	1.46	1.46	1.47	1.73	2.23	0.15	0.14	0.12	0.10	0.07	0.05	0.03	0.02	0.02	
(kg/m3)																		
rop1	0.002	0.002	0.002	0.003	0.003	0.31	3.23	4.88	17.56	11.84	8.80	6.79	4.33	2.99	2.28	2.04	2.05	
rop2	0.005	0.006	0.006	0.007	0.008	0.82	9.93	19.33	4.61	3.00	1.94	1.26	0.55	0.25	0.13	0.08	0.08	
rob1	0.001	0.001	0.001	0.001	0.001	0.15	1.50	2.24	52.37	59.85	67.33	74.81	89.77	104.73	119.69	134.66	138.40	
rop1 guess	1.00E+20	1.00E+20	1.00E+20	1.00E+20	1.00E+20	1.00E+20	1.00E+20	1.00E+20	1.00E+20	1.00E+20	1.00E+25	1.00E+25	1.00E+25	1.00E+25	1.00E+25	1.00E+25	1.00E+25	1.00E+25
rop2 guess	1.00E+20	1.00E+20	1.00E+20	1.00E+20	1.00E+20	1.00E+20	1.00E+20	1.00E+20	1.00E+20	1.00E+20	1.00E+25	1.00E+25	1.00E+25	1.00E+25	1.00E+25	1.00E+25	1.00E+25	1.00E+25
m	950	975	1000	1050	1100	1150	1375	1400	1450	1500	1525	1550	1650	1750	1850	2000	2100	2500
rob	4.75E+27	4.88E+27	5.00E+27	5.25E+27	5.50E+27	5.75E+27	6.88E+27	7.00E+27	7.25E+27	7.50E+27	7.63E+27	7.75E+27	8.25E+27	8.75E+27	9.25E+27	1.00E+28	1.05E+28	1.25E+28
rop1	7.05E+25	7.43E+25	8.04E+25	1.05E+26	1.71E+26	4.06E+26	5.43E+28	1.49E+28	1.17E+28	1.09E+28	1.07E+28	1.06E+28	1.08E+28	1.12E+28	1.17E+28	1.26E+28	1.32E+28	1.57E+28
rop2	1.37E+24	1.34E+24	1.36E+24	1.61E+24	2.43E+24	5.35E+24	1.65E+28	1.59E+28	1.26E+28	1.18E+28	1.16E+28	1.16E+28	1.17E+28	1.22E+28	1.28E+28	1.37E+28	1.44E+28	1.71E+28
potent	-2381	-2376	-2368	-2333	-2242	-1904	475700	116590	69236	59710	57984	57212	58831	63851	70471	82361	91382	135880
s	0.02	0.02	0.02	0.02	0.01	0.01	0.30	1.07	1.08	1.09	1.09	1.09	1.09	1.09	1.09	1.09	1.09	1.09
(kg/m3)																		
rop1	2.11	2.22	2.41	3.15	5.11	12.14	1625.57	445.98	349.96	325.06	320.18	317.88	321.77	334.58	350.56	376.95	395.23	470.34
rop2	0.07	0.07	0.07	0.09	0.13	0.28	876.82	845.90	671.92	627.61	619.20	615.47	624.31	649.42	680.44	731.30	766.58	911.40
rob1	142.14	145.88	149.62	157.10	164.58	172.06	205.72	209.47	216.95	224.43	228.17	231.91	246.87	261.83	276.79	299.24	314.20	374.05

Table 18: 1.8nm, esf1=0.0*k, esf2=74.22*k

sz	18																	
esf1	0																	
esf2	74.22																	
rop1 guess	1.00E+20	1.00E+20	1.00E+20	1.00E+20	1.00E+20	1.00E+20	1.00E+20	1.00E+20	1.00E+20	1.00E+20	1.00E+20	1.00E+20	1.00E+20	1.00E+20	1.00E+20	1.00E+20	1.00E+20	1.00E+20
rop2 guess	1.00E+20	1.00E+20	1.00E+20	1.00E+20	1.00E+20	1.00E+20	1.00E+20	1.00E+20	1.00E+20	1.00E+20	1.00E+20	1.00E+20	1.00E+20	1.00E+20	1.00E+20	1.00E+20	1.00E+20	1.00E+20
m	0.006	0.007	0.008	0.009	0.01	1	10	15	350	400	450	500	600	700	800	900	925	950
rob	3.00E+22	3.50E+22	4.00E+22	4.50E+22	5.00E+22	5.00E+24	5.00E+25	7.50E+25	1.75E+27	2.00E+27	2.25E+27	2.50E+27	3.00E+27	3.50E+27	4.00E+27	4.50E+27	4.63E+27	4.75E+27
rop1	3.00E+22	3.50E+22	4.00E+22	4.50E+22	5.00E+22	4.98E+24	4.80E+25	6.94E+25	1.88E+26	1.51E+26	1.21E+26	9.80E+25	6.55E+25	4.63E+25	3.57E+25	3.21E+25	3.24E+25	3.33E+25
rop2	9.13E+22	1.06E+23	1.22E+23	1.37E+23	1.52E+23	1.54E+25	1.89E+26	3.79E+26	9.71E+25	6.04E+25	3.83E+25	2.46E+25	1.06E+25	4.88E+24	2.51E+24	1.57E+24	1.46E+24	1.39E+24
potent	-2476	-2476	-2476	-2476	-2476	-2447	-2101	-1675	-2240	-2297	-2335	-2362	-2398	-2419	-2431	-2435	-2434	-2433
s	3.04	3.04	3.04	3.04	3.04	3.10	3.93	5.46	0.52	0.40	0.32	0.25	0.16	0.11	0.07	0.05	0.05	0.04
(kg/m3)																		
rop1	0.001	0.001	0.001	0.001	0.001	0.15	1.44	2.08	5.62	4.51	3.63	2.93	1.96	1.38	1.07	0.96	0.97	1.00
rop2	0.005	0.006	0.006	0.007	0.008	0.82	10.06	20.18	5.16	3.21	2.04	1.31	0.56	0.26	0.13	0.08	0.08	0.07
rob1	0.001	0.001	0.001	0.001	0.001	0.15	1.50	2.24	52.37	59.85	67.33	74.81	89.77	104.73	119.69	134.66	138.40	142.14
rop1 guess	1.00E+20	1.00E+20	1.00E+20	1.00E+20	1.00E+20	1.00E+20	1.00E+25	1.00E+25	1.00E+25	1.00E+25	1.00E+25	1.00E+25	1.00E+25	1.00E+25	1.00E+25	1.00E+25	1.00E+25	1.00E+25
rop2 guess	1.00E+20	1.00E+20	1.00E+20	1.00E+20	1.00E+20	1.00E+20	1.00E+25	1.00E+25	1.00E+25	1.00E+25	1.00E+25	1.00E+25	1.00E+25	1.00E+25	1.00E+25	1.00E+25	1.00E+25	1.00E+25
m	975	1000	1050	1100	1150	1175	1375	1400	1450	1500	1525	1550	1650	1750	1850	2000	2100	2500
rob	4.88E+27	5.00E+27	5.25E+27	5.50E+27	5.75E+27	5.88E+27	6.88E+27	7.00E+27	7.25E+27	7.50E+27	7.63E+27	7.75E+27	8.25E+27	8.75E+27	9.25E+27	1.00E+28	1.05E+28	1.25E+28
rop1	3.51E+25	3.80E+25	4.96E+25	7.99E+25	1.84E+26	3.53E+26	1.07E+28	1.50E+28	1.18E+28	1.10E+28	1.09E+28	1.08E+28	1.09E+28	1.14E+28	1.19E+28	1.28E+28	1.34E+28	1.58E+28
rop2	1.36E+24	1.39E+24	1.65E+24	2.54E+24	5.94E+24	1.13E+25	1.20E+28	1.59E+28	1.26E+28	1.18E+28	1.16E+28	1.16E+28	1.17E+28	1.22E+28	1.28E+28	1.37E+28	1.44E+28	1.71E+28
potent	-2430	-2426	-2411	-2370	-2228	-1992	1334400	117200	69924	60455	58751	57997	59664	64715	71361	83289	92335	136930
s	0.04	0.04	0.03	0.03	0.03	0.03	1.12	1.06	1.07	1.07	1.07	1.07	1.07	1.07	1.08	1.08	1.08	1.08
(kg/m3)																		
rop1	1.05	1.14	1.48	2.39	5.51	10.55	320.63	448.67	354.33	330.21	325.54	323.38	327.45	340.11	355.88	381.86	399.93	474.14
rop2	0.07	0.07	0.09	0.14	0.32	0.60	639.84	845.37	671.50	627.34	618.99	615.31	624.25	649.37	680.33	731.20	766.47	911.29
rob1	145.88	149.62	157.10	164.58	172.06	175.80	205.72	209.47	216.95	224.43	228.17	231.91	246.87	261.83	276.79	299.24	314.20	374.05

Table 19: 1.8nm, esf1=0.0*k, esf2=100.0*k

sz	18																		
esf1	0																		
esf2	100																		
rop1 guess	1.00E+20	1.00E+20	1.00E+20	1.00E+20	1.00E+20	1.00E+20	1.00E+20	1.00E+20	1.00E+20	1.00E+20	1.00E+20	1.00E+20	1.00E+20	1.00E+20	1.00E+20	1.00E+20	1.00E+20	1.00E+20	1.00E+20
rop2 guess	1.00E+20	1.00E+20	1.00E+20	1.00E+20	1.00E+20	1.00E+20	1.00E+20	1.00E+20	1.00E+20	1.00E+20	1.00E+20	1.00E+20	1.00E+20	1.00E+20	1.00E+20	1.00E+20	1.00E+20	1.00E+20	1.00E+20
m	0.006	0.007	0.008	0.009	0.01	1	10	275	300	325	350	400	450	500	600	700	800	900	925
rob	3.00E+22	3.50E+22	4.00E+22	4.50E+22	5.00E+22	5.00E+24	5.00E+25	1.38E+27	1.50E+27	1.63E+27	1.75E+27	2.00E+27	2.25E+27	2.50E+27	3.00E+27	3.50E+27	4.00E+27	4.50E+27	4.63E+27
rop1	3.00E+22	3.50E+22	4.00E+22	4.50E+22	5.00E+22	4.98E+24	4.57E+25	2.00E+27	2.27E+26	2.06E+26	1.86E+26	1.50E+26	1.21E+26	9.78E+25	6.55E+25	4.63E+25	3.57E+25	3.21E+25	3.24E+25
rop2	1.34E+23	1.57E+23	1.79E+23	2.02E+23	2.24E+23	2.30E+25	5.03E+26	1.19E+27	2.96E+26	2.10E+26	1.57E+26	9.34E+25	5.81E+25	3.69E+25	1.57E+25	7.20E+24	3.70E+24	2.31E+24	2.15E+24
potent	-2476	-2476	-2476	-2476	-2476	-2430	-1317	703	-1956	-2100	-2183	-2276	-2329	-2361	-2400	-2421	-2432	-2436	-2435
s	4.48	4.48	4.48	4.48	4.48	4.63	11.01	0.60	1.31	1.02	0.84	0.62	0.48	0.38	0.24	0.16	0.10	0.07	0.07
(kg/m3)																			
rop1	0.001	0.001	0.001	0.001	0.001	0.15	1.37	59.71	6.79	6.17	5.56	4.49	3.62	2.93	1.96	1.38	1.07	0.96	0.97
rop2	0.007	0.008	0.010	0.011	0.012	1.23	26.79	63.39	15.76	11.16	8.34	4.97	3.09	1.96	0.84	0.38	0.20	0.12	0.11
rob1	0.001	0.001	0.001	0.001	0.001	0.15	1.50	41.14	44.89	48.63	52.37	59.85	67.33	74.81	89.77	104.73	119.69	134.66	138.40
rop1 guess	1.00E+20	1.00E+20	1.00E+20	1.00E+20	1.00E+20	1.00E+20	1.00E+20	1.00E+20	1.00E+20	1.00E+20	1.00E+20	1.00E+22	1.00E+22	1.00E+22	1.00E+22	1.00E+22	1.00E+25	1.00E+25	1.00E+25
rop2 guess	1.00E+20	1.00E+20	1.00E+20	1.00E+20	1.00E+20	1.00E+20	1.00E+20	1.00E+20	1.00E+20	1.00E+20	1.00E+20	1.00E+22	1.00E+22	1.00E+22	1.00E+22	1.00E+22	1.00E+25	1.00E+25	1.00E+25
m	950	975	1000	1050	1100	1150	1175	1375	1400	1450	1500	1525	1550	1650	1750	1850	2000	2100	2500
rob	4.75E+27	4.88E+27	5.00E+27	5.25E+27	5.50E+27	5.75E+27	5.88E+27	6.88E+27	7.00E+27	7.25E+27	7.50E+27	7.63E+27	7.75E+27	8.25E+27	8.75E+27	9.25E+27	1.00E+28	1.05E+28	1.25E+28
rop1	3.33E+25	3.51E+25	3.80E+25	4.96E+25	7.99E+25	1.84E+26	3.52E+26	6.40E+28	1.50E+28	1.18E+28	1.11E+28	1.09E+28	1.08E+28	1.10E+28	1.14E+28	1.19E+28	1.27E+28	1.33E+28	1.58E+28
rop2	2.05E+24	2.01E+24	2.04E+24	2.42E+24	3.74E+24	8.76E+24	1.68E+25	5.81E+28	2.22E+28	1.87E+28	1.79E+28	1.78E+28	1.78E+28	1.82E+28	1.90E+28	1.99E+28	2.14E+28	2.24E+28	2.64E+28
potent	-2434	-2431	-2427	-2412	-2372	-2232	-2000	326750	143310	91472	82024	80725	80501	84998	93650	104550	124040	138920	213830
s	0.06	0.06	0.05	0.05	0.05	0.05	0.05	0.91	1.48	1.58	1.62	1.63	1.64	1.66	1.67	1.68	1.68	1.68	1.67
(kg/m3)																			
rop1	1.00	1.05	1.14	1.48	2.39	5.51	10.54	1916.40	448.29	354.30	330.69	326.20	324.10	327.99	340.23	355.64	381.26	399.18	473.21
rop2	0.11	0.11	0.11	0.13	0.20	0.47	0.89	3092.59	1178.81	992.43	951.41	946.04	945.82	970.19	1011.96	1060.16	1137.31	1190.14	1404.45
rob1	142.14	145.88	149.62	157.10	164.58	172.06	175.80	205.72	209.47	216.95	224.43	228.17	231.91	246.87	261.83	276.79	299.24	314.20	374.05

Table 20: 450nm, esf1=65.32*k, esf2=74.22*k

sz	4500																	
esf1	65.32																	
esf2	74.22																	
rop1 guess	1.00E+20	1.00E+20	1.00E+20	1.00E+20	1.00E+20	1.00E+20	1.00E+20	1.00E+20	1.00E+20	1.00E+20	1.00E+20	1.00E+20	1.00E+20	1.00E+20	1.00E+20	1.00E+20	1.00E+20	
rop2 guess	1.00E+20	1.00E+20	1.00E+20	1.00E+20	1.00E+20	1.00E+20	1.00E+20	1.00E+20	1.00E+20	1.00E+20	1.00E+20	1.00E+20	1.00E+20	1.00E+20	1.00E+20	1.00E+20	1.00E+20	
m	0.006	0.007	0.008	0.009	0.01	1	10	15	350	400	450	500	600	700	800	900	925	
rob	3.00E+22	3.50E+22	4.00E+22	4.50E+22	5.00E+22	5.00E+24	5.00E+25	7.50E+25	1.75E+27	2.00E+27	2.25E+27	2.50E+27	3.00E+27	3.50E+27	4.00E+27	4.50E+27	4.63E+27	
rop1	3.01E+22	3.51E+22	4.01E+22	4.51E+22	5.01E+22	5.01E+24	5.01E+25	7.51E+25	2.08E+26	1.62E+26	1.28E+26	1.02E+26	6.73E+25	4.72E+25	3.63E+25	3.25E+25	3.28E+25	
rop2	3.01E+22	3.51E+22	4.01E+22	4.51E+22	5.01E+22	4.99E+24	4.73E+25	6.86E+25	2.84E+25	1.85E+25	1.21E+25	7.90E+24	3.45E+24	1.60E+24	8.27E+23	5.16E+23	4.80E+23	
potent	-2476	-2476	-2476	-2476	-2476	-2468	-2391	-2350	-2145	-2215	-2267	-2308	-2363	-2396	-2414	-2420	-2419	
s	1.00	1.00	1.00	1.00	1.00	1.00	0.94	0.91	0.14	0.11	0.09	0.08	0.05	0.03	0.02	0.02	0.01	
(kg/m3)																		
rop1	0.001	0.001	0.001	0.001	0.001	0.15	1.50	2.25	6.22	4.86	3.83	3.06	2.01	1.41	1.09	0.97	0.98	
rop2	0.002	0.002	0.002	0.002	0.003	0.27	2.52	3.65	1.51	0.99	0.64	0.42	0.18	0.09	0.04	0.03	0.03	
rob1	0.001	0.001	0.001	0.001	0.001	0.15	1.50	2.24	52.37	59.85	67.33	74.81	89.77	104.73	119.69	134.66	138.40	
rop1 guess	1.00E+20	1.00E+20	1.00E+20	1.00E+20	1.00E+20	1.00E+20	1.00E+20	1.00E+20	1.00E+22	1.00E+22	1.00E+22	1.00E+22	1.00E+22	1.00E+22	1.00E+22	1.00E+22	1.00E+22	1.00E+22
rop2 guess	1.00E+20	1.00E+20	1.00E+20	1.00E+20	1.00E+20	1.00E+20	1.00E+20	1.00E+20	1.00E+22	1.00E+22	1.00E+22	1.00E+22	1.00E+22	1.00E+22	1.00E+22	1.00E+22	1.00E+22	1.00E+22
m	950	975	1000	1050	1100	1150	1375	1400	1450	1500	1525	1550	1650	1750	1850	2000	2100	2500
rob	4.75E+27	4.88E+27	5.00E+27	5.25E+27	5.50E+27	5.75E+27	6.88E+27	7.00E+27	7.25E+27	7.50E+27	7.63E+27	7.75E+27	8.25E+27	8.75E+27	9.25E+27	1.00E+28	1.05E+28	1.25E+28
rop1	3.38E+25	3.56E+25	3.86E+25	5.06E+25	8.24E+25	1.98E+26	5.73E+28	1.29E+28	9.86E+27	9.05E+27	8.88E+27	8.79E+27	8.82E+27	9.12E+27	9.52E+27	1.02E+28	1.07E+28	1.27E+28
rop2	4.58E+23	4.49E+23	4.57E+23	5.42E+23	8.34E+23	1.94E+24	5.99E+28	1.88E+28	1.54E+28	1.45E+28	1.44E+28	1.43E+28	1.46E+28	1.51E+28	1.58E+28	1.69E+28	1.77E+28	2.09E+28
potent	-2417	-2414	-2409	-2387	-2331	-2121	336020	125550	76964	67448	65808	65139	67235	72822	80107	93169	103080	151920
s	0.01	0.01	0.01	0.01	0.01	0.01	1.04	1.46	1.56	1.60	1.62	1.63	1.65	1.66	1.66	1.66	1.66	1.65
(kg/m3)																		
rop1	1.01	1.07	1.15	1.51	2.47	5.93	1715.55	386.28	295.05	270.93	265.85	263.13	263.99	272.92	284.85	305.10	319.37	378.56
rop2	0.02	0.02	0.02	0.03	0.04	0.10	3185.54	1002.17	817.92	772.96	765.14	762.21	775.36	805.47	841.86	901.29	942.37	1110.12
rob1	142.14	145.88	149.62	157.10	164.58	172.06	205.72	209.47	216.95	224.43	228.17	231.91	246.87	261.83	276.79	299.24	314.20	374.05

Table 21: 450nm, esf1=0.0*k, esf2=74.22*k

sz	4500																	
esf1	0																	
esf2	74.22																	
rop1 guess	1.00E+20	1.00E+20	1.00E+20	1.00E+20	1.00E+20	1.00E+20	1.00E+20	1.00E+20	1.00E+20	1.00E+20	1.00E+20	1.00E+20	1.00E+20	1.00E+20	1.00E+20	1.00E+20	1.00E+20	1.00E+20
rop2 guess	1.00E+20	1.00E+20	1.00E+20	1.00E+20	1.00E+20	1.00E+20	1.00E+20	1.00E+20	1.00E+20	1.00E+20	1.00E+20	1.00E+20	1.00E+20	1.00E+20	1.00E+20	1.00E+20	1.00E+20	1.00E+20
m	0.006	0.007	0.008	0.009	0.01	1	10	15	350	400	450	500	600	700	800	900	925	950
rob	3.00E+22	3.50E+22	4.00E+22	4.50E+22	5.00E+22	5.00E+24	5.00E+25	7.50E+25	1.75E+27	2.00E+27	2.25E+27	2.50E+27	3.00E+27	3.50E+27	4.00E+27	4.50E+27	4.63E+27	4.75E+27
rop1	3.00E+22	3.50E+22	4.00E+22	4.50E+22	5.00E+22	5.00E+24	5.00E+25	7.49E+25	2.07E+26	1.62E+26	1.28E+26	1.02E+26	6.72E+25	4.71E+25	3.62E+25	3.25E+25	3.28E+25	3.37E+25
rop2	3.01E+22	3.51E+22	4.01E+22	4.51E+22	5.01E+22	4.99E+24	4.73E+25	6.86E+25	2.84E+25	1.85E+25	1.21E+25	7.90E+24	3.45E+24	1.60E+24	8.27E+23	5.16E+23	4.80E+23	4.58E+23
potent	-2476	-2476	-2476	-2476	-2476	-2468	-2391	-2350	-2146	-2215	-2268	-2308	-2363	-2396	-2414	-2420	-2419	-2417
s	1.00	1.00	1.00	1.00	1.00	1.00	0.95	0.92	0.14	0.11	0.09	0.08	0.05	0.03	0.02	0.02	0.01	0.01
(kg/m3)																		
rop1	0.001	0.001	0.001	0.001	0.001	0.15	1.50	2.24	6.21	4.84	3.82	3.05	2.01	1.41	1.08	0.97	0.98	1.01
rop2	0.002	0.002	0.002	0.002	0.003	0.27	2.52	3.65	1.51	0.99	0.64	0.42	0.18	0.09	0.04	0.03	0.03	0.02
rob1	0.001	0.001	0.001	0.001	0.001	0.15	1.50	2.24	52.37	59.85	67.33	74.81	89.77	104.73	119.69	134.66	138.40	142.14
rop1 guess	1.00E+20	1.00E+20	1.00E+20	1.00E+20	1.00E+20	1.00E+20	1.00E+20	1.00E+20	1.00E+25	1.00E+25	1.00E+25	1.00E+25	1.00E+25	1.00E+25	1.00E+25	1.00E+25	1.00E+25	1.00E+25
rop2 guess	1.00E+20	1.00E+20	1.00E+20	1.00E+20	1.00E+20	1.00E+20	1.00E+20	1.00E+20	1.00E+25	1.00E+25	1.00E+25	1.00E+25	1.00E+25	1.00E+25	1.00E+25	1.00E+25	1.00E+25	1.00E+25
m	975	1000	1050	1100	1150	1175	1375	1400	1450	1500	1525	1550	1650	1750	1850	2000	2100	2500
rob	4.88E+27	5.00E+27	5.25E+27	5.50E+27	5.75E+27	5.88E+27	6.88E+27	7.00E+27	7.25E+27	7.50E+27	7.63E+27	7.75E+27	8.25E+27	8.75E+27	9.25E+27	1.00E+28	1.05E+28	1.25E+28
rop1	3.55E+25	3.85E+25	5.05E+25	8.22E+25	1.98E+26	2.38E+27	5.73E+28	1.29E+28	9.86E+27	9.05E+27	8.88E+27	8.79E+27	8.82E+27	9.12E+27	9.52E+27	1.02E+28	1.07E+28	1.27E+28
rop2	4.49E+23	4.57E+23	5.42E+23	8.34E+23	1.94E+24	1.30E+24	5.99E+28	1.88E+28	1.54E+28	1.45E+28	1.44E+28	1.43E+28	1.46E+28	1.51E+28	1.58E+28	1.69E+28	1.77E+28	2.09E+28
potent	-2414	-2409	-2388	-2331	-2122	3005	336020	125550	76965	67450	65810	65141	67237	72824	80109	93171	103080	151920
s	0.01	0.01	0.01	0.01	0.01	0.00	1.04	1.46	1.56	1.60	1.62	1.63	1.65	1.66	1.66	1.66	1.66	1.65
(kg/m3)																		
rop1	1.06	1.15	1.51	2.46	5.91	71.22	1715.55	386.28	295.06	270.94	265.87	263.14	264.00	272.93	284.87	305.13	319.37	378.56
rop2	0.02	0.02	0.03	0.04	0.10	0.07	3185.48	1002.22	817.92	773.01	765.14	762.21	775.36	805.47	841.86	901.29	942.37	1110.12
rob1	145.88	149.62	157.10	164.58	172.06	175.80	205.72	209.47	216.95	224.43	228.17	231.91	246.87	261.83	276.79	299.24	314.20	374.05

Table 22: 450nm, esf1=0.0*k, esf2=100.0*k

sz	4500																		
esf1	0																		
esf2	100																		
rop1 guess	1.00E+20	1.00E+20	1.00E+20	1.00E+20	1.00E+20	1.00E+20	1.00E+20	1.00E+20	1.00E+20	1.00E+20	1.00E+20	1.00E+20	1.00E+20	1.00E+20	1.00E+20	1.00E+20	1.00E+20	1.00E+20	1.00E+20
rop2 guess	1.00E+20	1.00E+20	1.00E+20	1.00E+20	1.00E+20	1.00E+20	1.00E+20	1.00E+20	1.00E+20	1.00E+20	1.00E+20	1.00E+20	1.00E+20	1.00E+20	1.00E+20	1.00E+20	1.00E+20	1.00E+20	1.00E+20
m	0.006	0.007	0.008	0.009	0.01	1	10	275	300	325	350	400	450	500	600	700	800	900	925
rob	3.00E+22	3.50E+22	4.00E+22	4.50E+22	5.00E+22	5.00E+24	5.00E+25	1.38E+27	1.50E+27	1.63E+27	1.75E+27	2.00E+27	2.25E+27	2.50E+27	3.00E+27	3.50E+27	4.00E+27	4.50E+27	4.63E+27
rop1	3.00E+22	3.50E+22	4.00E+22	4.50E+22	5.00E+22	5.00E+24	5.00E+25	3.10E+26	2.70E+26	2.36E+26	2.07E+26	1.62E+26	1.28E+26	1.02E+26	6.72E+25	4.71E+25	3.62E+25	3.25E+25	3.28E+25
rop2	3.01E+22	3.51E+22	4.02E+22	4.52E+22	5.02E+22	4.99E+24	4.73E+25	5.30E+25	4.32E+25	3.51E+25	2.84E+25	1.86E+25	1.21E+25	7.91E+24	3.46E+24	1.60E+24	8.28E+23	5.17E+23	4.81E+23
potent	-2476	-2476	-2476	-2476	-2476	-2468	-2391	-1989	-2051	-2102	-2146	-2215	-2268	-2308	-2363	-2396	-2414	-2420	-2419
s	1.00	1.00	1.00	1.00	1.00	1.00	0.95	0.17	0.16	0.15	0.14	0.11	0.09	0.08	0.05	0.03	0.02	0.02	0.01
(kg/m3)																			
rop1	0.001	0.001	0.001	0.001	0.001	0.15	1.50	9.27	8.07	7.06	6.21	4.84	3.82	3.05	2.01	1.41	1.08	0.97	0.98
rop2	0.002	0.002	0.002	0.002	0.003	0.27	2.52	2.82	2.30	1.86	1.51	0.99	0.64	0.42	0.18	0.09	0.04	0.03	0.03
rob1	0.001	0.001	0.001	0.001	0.001	0.15	1.50	41.14	44.89	48.63	52.37	59.85	67.33	74.81	89.77	104.73	119.69	134.66	138.40
rop1 guess	1.00E+20	1.00E+20	1.00E+20	1.00E+20	1.00E+20	1.00E+20	1.00E+20	1.00E+20	1.00E+20	1.00E+22	1.00E+22	1.00E+22	1.00E+22	1.00E+22	1.00E+22	1.00E+22	1.00E+22	1.00E+22	1.00E+22
rop2 guess	1.00E+20	1.00E+20	1.00E+20	1.00E+20	1.00E+20	1.00E+20	1.00E+20	1.00E+20	1.00E+20	1.00E+22	1.00E+22	1.00E+22	1.00E+22	1.00E+22	1.00E+22	1.00E+22	1.00E+22	1.00E+22	1.00E+22
m	950	975	1000	1050	1100	1150	1175	1375	1400	1450	1500	1525	1550	1650	1750	1850	2000	2100	2500
rob	4.75E+27	4.88E+27	5.00E+27	5.25E+27	5.50E+27	5.75E+27	5.88E+27	6.88E+27	7.00E+27	7.25E+27	7.50E+27	7.63E+27	7.75E+27	8.25E+27	8.75E+27	9.25E+27	1.00E+28	1.05E+28	1.25E+28
rop1	3.37E+25	3.55E+25	3.85E+25	5.05E+25	8.22E+25	1.98E+26	2.38E+27	5.73E+28	1.29E+28	9.86E+27	9.05E+27	8.88E+27	8.79E+27	8.82E+27	9.12E+27	9.52E+27	1.02E+28	1.07E+28	1.27E+28
rop2	4.58E+23	4.50E+23	4.57E+23	5.42E+23	8.35E+23	1.94E+24	1.30E+24	5.99E+28	1.88E+28	1.54E+28	1.45E+28	1.44E+28	1.43E+28	1.46E+28	1.51E+28	1.58E+28	1.69E+28	1.77E+28	2.09E+28
potent	-2417	-2414	-2409	-2388	-2331	-2122	3005	336020	125550	76964	67448	65809	65139	67236	72822	80107	93169	103080	151920
s	0.01	0.01	0.01	0.01	0.01	0.01	0.00	1.04	1.46	1.56	1.60	1.62	1.63	1.65	1.66	1.66	1.66	1.66	1.65
(kg/m3)																			
rop1	1.01	1.06	1.15	1.51	2.46	5.91	71.22	1715.55	386.28	295.06	270.94	265.87	263.14	264.00	272.93	284.87	305.13	319.37	378.56
rop2	0.02	0.02	0.02	0.03	0.04	0.10	0.07	3185.43	1002.17	817.92	772.96	765.14	762.21	775.36	805.47	841.86	901.29	942.31	1110.12
rob1	142.14	145.88	149.62	157.10	164.58	172.06	175.80	205.72	209.47	216.95	224.43	228.17	231.91	246.87	261.83	276.79	299.24	314.20	374.05

Table 23: 220nm, esf1= 0.0*k, esf2=75.22*k

rop1 guess= 1e20								rop1guess= 1e25														
rop2 guess= 1e20								rop2guess=1e26														
m	0.006	0.007	0.008	0.009	0.01	1	10	100	500	900	925	950	975	1000	1050	1100	1200	1400	1425	1450	1500	2000
s	1.006	1.006	1.006	1.006	1.006	1.006	1.006	1.0961	0.0785	0.016	0.0147	0.0136	0.0127	0.0119	0.0108	0.0102	1.3566	0.9997	0.9992	0.9993	0.9997	1.0001
rop1	3.00E+22	3.50E+22	4.00E+22	4.50E+22	5.00E+22	9.99E+23	4.99E+25	4.68E+26	1.02E+26	3.25E+25	3.28E+25	3.37E+25	3.55E+25	3.85E+25	5.04E+25	8.22E+25	2.55E+27	1.29E+28	1.08E+28	9.80E+27	8.86E+27	1.02E+28
rop2	3.02E+22	3.52E+22	4.02E+22	4.53E+22	5.03E+22	5.03E+24	5.02E+25	5.13E+26	8.00E+24	5.18E+23	4.82E+23	4.59E+23	4.51E+23	4.59E+23	5.44E+23	8.37E+23	3.46E+27	1.29E+28	1.08E+28	9.79E+27	8.85E+27	1.02E+28
rob1	3.00E+22	3.50E+22	4.00E+22	4.50E+22	5.00E+22	5.00E+24	5.00E+25	5.00E+26	2.50E+27	4.50E+27	4.63E+27	4.75E+27	4.88E+27	5.00E+27	5.25E+27	5.50E+27	6.00E+27	7.00E+27	7.13E+27	7.25E+27	7.50E+27	1.00E+28
rob2	3.00E+22	3.50E+22	4.00E+22	4.50E+22	5.00E+22	5.00E+24	5.00E+25	5.00E+26	2.50E+27	4.50E+27	4.63E+27	4.75E+27	4.88E+27	5.00E+27	5.25E+27	5.50E+27	6.00E+27	7.00E+27	7.13E+27	7.25E+27	7.50E+27	1.00E+28
potent	-2476	-2476	-2476	-2476	-2476	-2464	-2355	-1196	-2308	-2420	-2419	-2417	-2414	-2409	-2388	-2331	8508	103970	71433	58928	48507	63225
(kg/m3)																						
rop1	0.001	0.001	0.001	0.001	0.001	0.03	1.49	14.00	3.05	0.97	0.98	1.01	1.06	1.15	1.51	2.46	76.39	386.64	323.00	293.20	265.02	303.72
rop2	0.002	0.002	0.002	0.002	0.003	0.27	2.67	27.28	0.43	0.03	0.03	0.02	0.02	0.02	0.03	0.04	184.26	687.25	573.82	520.95	471.06	540.08
rob1	0.001	0.001	0.001	0.001	0.001	0.15	1.50	14.96	74.81	134.66	138.40	142.14	145.88	149.62	157.10	164.58	179.54	209.47	213.21	216.95	224.43	299.24
rob2	0.002	0.002	0.002	0.002	0.003	0.27	2.66	26.60	133.01	239.42	246.07	252.72	259.37	266.02	279.33	292.63	319.23	372.43	379.09	385.74	399.04	532.05

Table 24: 100nm, esf1= 0.0*k, esf2=75.22*k

rop1 guess = 1e20								rop1guess= 1e25														
rop2 guess = 1e20								rop2guess=1e26														
m	0.006	0.007	0.008	0.009	0.01	1	10	100	500	900	925	950	975	1000	1050	1100	1400	1425	1450	1500	2000	
s	1.0133	1.0133	1.0133	1.0133	1.0133	1.0134	1.0144	1.0781	0.0791	0.0161	0.0148	0.0137	0.0128	0.012	0.0109	0.0103	0.9997	0.9992	0.9993	0.9997	1.0002	
rop1	3.00E+22	3.50E+22	4.00E+22	4.50E+22	5.00E+22	5.00E+24	4.99E+25	4.68E+26	1.02E+26	3.25E+25	3.28E+25	3.37E+25	3.55E+25	3.85E+25	5.04E+25	8.22E+25	1.29E+28	1.08E+28	9.81E+27	8.87E+27	1.02E+28	
rop2	3.04E+22	3.55E+22	4.05E+22	4.56E+22	5.07E+22	5.07E+24	5.06E+25	5.05E+26	8.06E+24	5.22E+23	4.85E+23	4.63E+23	4.54E+23	4.62E+23	5.48E+23	8.43E+23	1.29E+28	1.08E+28	9.80E+27	8.87E+27	1.02E+28	
rob1	3.00E+22	3.50E+22	4.00E+22	4.50E+22	5.00E+22	5.00E+24	5.00E+25	5.00E+26	2.50E+27	4.50E+27	4.63E+27	4.75E+27	4.88E+27	5.00E+27	5.25E+27	5.50E+27	7.00E+27	7.13E+27	7.25E+27	7.50E+27	1.00E+28	
rob2	3.00E+22	3.50E+22	4.00E+22	4.50E+22	5.00E+22	5.00E+24	5.00E+25	5.00E+26	2.50E+27	4.50E+27	4.63E+27	4.75E+27	4.88E+27	5.00E+27	5.25E+27	5.50E+27	7.00E+27	7.13E+27	7.25E+27	7.50E+27	1.00E+28	
potent	-2476	-2476	-2476	-2476	-2476	-2464	-2355	-1215	-2308	-2420	-2419	-2418	-2414	-2409	-2388	-2331	104030	71478	58973	48566	63305	
(kg/m3)																						
rop1	0.001	0.001	0.001	0.001	0.001	0.15	1.49	14.01	3.05	0.97	0.98	1.01	1.06	1.15	1.51	2.46	323.32	323.32	293.52	265.40	304.11	
rop2	0.002	0.002	0.002	0.002	0.003	0.27	2.69	26.86	0.43	0.03	0.03	0.02	0.02	0.02	0.03	0.04	574.40	574.40	521.55	471.73	540.83	
rob1	0.001	0.001	0.001	0.001	0.001	0.15	1.50	14.96	74.81	134.66	138.40	142.14	145.88	149.62	157.10	164.58	209.47	213.21	216.95	224.43	299.24	
rob2	0.002	0.002	0.002	0.002	0.003	0.27	2.66	26.60	133.01	239.42	246.07	252.72	259.37	266.02	279.33	292.63	372.43	379.09	385.74	399.04	532.05	